

See discussions, stats, and author profiles for this publication at: <https://www.researchgate.net/publication/231440161>

# The Reaction of Zinc, Cadmium, and Mercury Atoms with Methane: Infrared Spectra of the Matrix-Isolated Methylmetal Hydrides

ARTICLE *in* JOURNAL OF THE AMERICAN CHEMICAL SOCIETY · APRIL 2002

Impact Factor: 12.11 · DOI: 10.1021/ja00136a015

---

CITATIONS

38

---

READS

14

3 AUTHORS, INCLUDING:



[Anthony J Downs](#)

University of Oxford

258 PUBLICATIONS 5,007 CITATIONS

SEE PROFILE

# Thermal and Photochemical Reactions of Aluminum, Gallium, and Indium Atoms (M) in the Presence of Ammonia: Generation and Characterization of the Species $M\cdot NH_3$ , $HMNH_2$ , $MNH_2$ , and $H_2MNH_2$

Hans-Jörg Himmel,\* Anthony J. Downs, and Tim M. Greene

Contribution from the Inorganic Chemistry Laboratory, University of Oxford, South Parks Road, Oxford OX1 3QR, U.K.

Received April 14, 2000

**Abstract:** Isolation of aluminum, gallium, and indium atoms together with ammonia in a solid argon matrix is shown to result in a thermal reaction yielding the metal atom complex  $Al\cdot NH_3$ ,  $Ga\cdot NH_3$ , or  $In\cdot NH_3$ , which has been characterized by its IR and UV–visible spectra. Upon photoactivation at  $\lambda = 436$  nm, the metal atom inserts into an N–H bond of ammonia to form the divalent compound  $HMNH_2$  ( $M = Al, Ga, \text{ or } In$ ). This product is photolabile, decomposing to the corresponding monovalent compound  $MNH_2$  on exposure to broad-band UV–visible light ( $200 \leq \lambda \leq 800$  nm). All the molecules have been identified by means of their IR spectra, the assignments being underwritten by the effects of D and  $^{15}N$  substitution, and also by comparison either with the vibrational properties of known, related molecules or with those predicted by quantum chemical (DFT) calculations. The resulting analysis is elaborated for the light it sheds on the structures and electronic properties of the molecules.

## Introduction

Compounds containing the group 13 metals bound to nitrogen are potentially relevant to the fabrication of the III–V semiconductor materials  $AlN$ ,  $GaN$ , and  $InN$ .<sup>1</sup> In practice, these materials are made by organometallic chemical vapor deposition (OMCVD) processes starting from sources such as  $Ga(CH_3)_3$  and  $NH_3$ .<sup>1</sup> The vapors of the precursors in  $H_2$  as the carrier gas react at high temperatures at the substrate surface with the deposition of the metal nitride. Since hydrogen is one of the main impurities in the bulk material, the influence of hydrogen on the properties of the semiconductor device has been the subject of no little study.<sup>2</sup> The decomposition process is likely to proceed by way of intermediates with the composition  $H_xM_yN_z$  ( $M = Al, Ga, \text{ or } In$ ); indeed the specific compounds amidogallane,  $[H_2GaNH_2]_3$ ,<sup>3</sup> and azidogallane,  $[H_2GaN_3]_n$ ,<sup>4</sup> are reported to be ready sources of  $GaN$  in cubic nanocrystalline form and thin films, respectively. Studies of a

different kind involving high-resolution electron loss spectroscopy (HREELS), low energy electron diffraction (LEED), and other techniques show that adsorption of hydrogen atoms results in the creation on the  $GaN$  (0001) surface of  $Ga-H$  bonds that are destroyed only on heating to temperatures of 260 °C or higher.<sup>5</sup> It follows that detailed investigation of species with the general formula  $H_xM_yN_z$  may be expected to illuminate our understanding not only of the decomposition processes implicated in the OMCVD formation of the binary nitride  $MN$ , but also of the factors affecting the properties of the product.

Matrix isolation is now well established as a highly instructive method of reconnaissance and characterization for previously unknown hydride derivatives of the group 13 metals.<sup>6,7</sup> Hence, for example, the simple monomeric molecule amidoborane,  $H_2BNH_2$ , has been identified as a product arising from the pyrolysis of mixtures of diborane and ammonia.<sup>8,9</sup> Moreover, the reactions of the metal atoms with dihydrogen molecules or hydrogen atoms have been shown to afford the first clear sighting of the binary hydride molecules  $MH$ ,  $MH_2$ , and  $MH_3$  ( $M = Al, Ga, \text{ or } In$ ).<sup>10</sup> Photoexcitation of the metal atoms is needed to promote insertion not only into the H–H bond of dihydrogen to give  $MH_2$ ,<sup>10</sup> but also into a C–H bond of methane

\* To whom correspondence should be addressed.

(1) Downs, A. J., Ed. *Chemistry of Aluminium, Gallium, Indium and Thallium*; Blackie: Glasgow, U.K., 1993. Edgar, J. H., Ed. *Properties of Group III Nitrides*; EMIS: London, U.K., 1994.

(2) Yu, Z.; Buczkowski, S. L.; Giles, N. C.; Myers, T. H.; Richards-Babb, M. R. *Appl. Phys. Lett.* **1996**, 69, 2731–2733. Han, J.; Ng, T.-B.; Biefeld, R. M.; Crawford, M. H.; Follstaedt, D. M. *Appl. Phys. Lett.* **1997**, 71, 3114–3116. Koleske, D. D.; Wickenden, A. E.; Henry, R. L.; Twigg, M. E.; Culbertson, J. C.; Gorman, R. J. *Appl. Phys. Lett.* **1998**, 73, 2018–2020. Nakamura, S.; Iwasa, N.; Senoh, M.; Mukai, T. *Jpn. J. Appl. Phys., Part 1* **1992**, 31, 1258–1266. Pearton, S. J.; Abernathy, C. R.; Ren, F.; Lothian, J. R.; Wisk, P. W.; Katz, A.; Constantine, C. *Semicond. Sci. Technol.* **1993**, 8, 310–312.

(3) Hwang, J.-W.; Campbell, J. P.; Kozubowski, J.; Hanson, S. A.; Evans, J. F.; Gladfelter, W. L. *Chem. Mater.* **1995**, 7, 517–525. Campbell, J. P.; Hwang, J.-W.; Young, V. G., Jr.; Von Dreele, R. B.; Cramer, C. J.; Gladfelter, W. L. *J. Am. Chem. Soc.* **1998**, 120, 521–531.

(4) McMurran, J.; Kouvetakis, J.; Nesting, D. C.; Smith, D. J.; Hubbard, J. L. *J. Am. Chem. Soc.* **1998**, 120, 5233–5237. McMurran, J.; Dai, D.; Balasubramanian, K.; Steffek, C.; Kouvetakis, J.; Hubbard, J. L. *Inorg. Chem.* **1998**, 37, 6638–6644.

(5) Bellitto, V. J.; Thoms, B. D.; Koleske, D. D.; Wickenden, A. E.; Henry, R. L. *Surf. Sci.* **1999**, 430, 80–88. Bellitto, V. J.; Yang, Y.; Thoms, B. D.; Koleske, D. D.; Wickenden, A. E.; Henry, R. L. *Surf. Sci.* **1999**, 442, L1019–L1023.

(6) Almond, M. J.; Downs, A. J. *Adv. Spectrosc.* **1989**, 17, 1–511. Downs, A. J.; Greene, T. M. *Adv. Inorg. Chem.* **1998**, 46, 101–171.

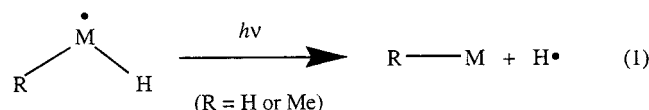
(7) Downs, A. J. *Coord. Chem. Rev.* **1999**, 189, 59–100.

(8) Carpenter, J. D.; Ault, B. S. *J. Phys. Chem.* **1991**, 95, 3502–3506; *Chem. Phys. Lett.* **1992**, 197, 171–174. Sugie, M.; Takeo, H.; Matsumura, C. *Chem. Phys. Lett.* **1979**, 64, 573–575.

(9) McKee, M. L. *J. Phys. Chem.* **1992**, 96, 5380–5385.

(10) Pullumbi, P.; Mijoule, C.; Manceron, L.; Bouteiller, Y. *Chem. Phys.* **1994**, 185, 13–24. Pullumbi, P.; Bouteiller, Y.; Manceron, L.; Mijoule, C. *Chem. Phys.* **1994**, 185, 25–37.

to give  $\text{CH}_3\text{MH}$  ( $\text{M} = \text{Al}$ ,<sup>11</sup>  $\text{Ga}$ <sup>12–14</sup> or  $\text{In}$ <sup>14</sup>); these divalent products are themselves photolabile, decomposing with the release of H atoms and the formation of the appropriate monovalent derivative (eq 1). The only insertion reactions of gallium and indium that have been found to proceed *without* photoactivation are those with HCl to give MCl and MH ( $\text{M} = \text{Ga}$  or  $\text{In}$ , although MH could be detected only for  $\text{M} = \text{Ga}$ )<sup>15</sup> and  $\text{H}_2$ , which reacts spontaneously with the  $\text{Ga}_2$  dimer to give the hydrido-bridged species  $\text{Ga}(\mu\text{-H})_2\text{Ga}$ .<sup>13,16,17</sup>



Here we report on the outcome of the reactions set in train by thermal or photolytic excitation of gallium or indium atoms isolated in ammonia-doped argon matrices. Previous studies of the reactions occurring between aluminum and ammonia in solid adamantane or argon matrices have been guided by EPR<sup>18</sup> or IR<sup>19</sup> measurements, respectively. The EPR experiments find evidence of the adducts  $\text{Al}(\text{NH}_3)_2$  and  $\text{Al}(\text{NH}_3)_4$  and what was thought to be the insertion product  $\text{HAlNH}_2$ , apparently featuring a bridging hydrogen atom, all formed by thermal reactions of ground-state Al atoms.<sup>18</sup> On the evidence of the IR experiments, Al atoms produced by laser ablation (and therefore including a proportion of electronically excited atoms) react with  $\text{NH}_3$  to form two major products  $\text{HAlNH}_2$  and  $\text{AlNH}_2$ , as well as another minor product tentatively identified as  $\text{HAlNH}$ .<sup>19</sup> These experiments indicated too that electronic excitation of the Al atoms is a prerequisite to insertion into an N–H bond of the  $\text{NH}_3$  molecule, while offering no suggestion that the primary product  $\text{HAlNH}_2$  carries other than terminal Al–H and N–H bonds. Photodecomposition of  $\text{HAlNH}_2$  is then the source of the other two products. EPR studies of the reaction of Li atoms with  $\text{NH}_3$  have identified the formation of the molecular complex  $\text{Li}\cdot\text{NH}_3$ , which decomposes under the action of visible light, possibly with the formation of  $\text{LiNH}_2$  and  $\text{LiNH}$ , although these could not be positively identified.<sup>20</sup> Matrix methods have also been used to investigate the reactions of certain transition metals with ammonia. Thus,  $\text{Fe}$ <sup>21</sup> and  $\text{Ni}$ <sup>22</sup> atoms severally form adducts with one or two molecules of  $\text{NH}_3$ , and UV irradiation brings about insertion of the metal into an N–H bond with the formation of the amido derivatives  $\text{HMNH}_2$  and  $\text{HMNH}_2\cdot\text{NH}_3$  ( $\text{M} = \text{Fe}$  or  $\text{Ni}$ ).

Ammonia complexes and amido and imido derivatives of aluminum have attracted several quantum chemical inquiries designed to elucidate the ground-state structures, vibrational properties, energetics, and, in particular, the bonding in such molecules.<sup>7,23–28</sup> As expected, the adducts  $\text{Al}\cdot\text{NH}_3$ <sup>23,24</sup> and  $\text{H}_3\text{Al}\cdot\text{NH}_3$ <sup>24,25</sup> are calculated to differ markedly in their binding energies (27–40 vs ca. 110  $\text{kJ mol}^{-1}$ ) and Al–N distances (2.350 vs 2.072 Å).  $\text{Al}\cdot\text{NH}_3$  is noteworthy on two counts: (i) it is subject to Jahn–Teller distortion, albeit with minimal perturbation of the geometry and vibrational properties of the molecule (reflecting the highly localized character of the semioccupied orbital), and (ii) it is 110  $\text{kJ}$  less stable than its tautomer  $\text{HAlNH}_2$ .<sup>24</sup> With a planar structure and a relatively short Al–N bond (1.772 Å),  $\text{HAlNH}_2$  represents the global minimum for molecules with the composition  $\text{AlNH}_3$ . The most stable  $\text{AlNH}_2$  isomer is not the quasi-linear  $\text{HAlNH}$  but the planar aluminum(I) species  $\text{AlNH}_2$ , also with a surprisingly short Al–N bond (1.795 Å);<sup>24</sup> together with an H atom this is formed from  $\text{HAlNH}_2$  in a reaction analogous to eq 1 that is estimated to be exothermic by about 170  $\text{kJ mol}^{-1}$ . Shortest of all are the Al–N bonds in the high-energy  $\text{HAlNH}$  (1.608 Å)<sup>24–27</sup> and the low-energy, planar  $\text{H}_2\text{AlNH}_2$  molecule (1.766 Å)<sup>24–26</sup> for which the barrier to rotation about the Al–N bond is calculated<sup>28</sup> to be 45–60  $\text{kJ mol}^{-1}$  (cf. 160  $\text{kJ mol}^{-1}$  for  $\text{H}_2\text{BNH}_2$ <sup>9</sup>). There are signs therefore suggesting a degree of multiple bonding, but the precise nature and importance of such bonding are open to question.<sup>7,29</sup> Beyond doubt, however, is the need for more experimental facts not only about these, but also about the corresponding derivatives of gallium and indium, virtually uncharted up to the present time.

We will show that aluminum, gallium, and indium atoms in their <sup>2</sup>P ground states form relatively well-defined complexes  $\text{M}\cdot\text{NH}_3$  ( $\text{M} = \text{Al}$ ,  $\text{Ga}$ , or  $\text{In}$ ) on co-condensation with ammonia. The complexes are characterized by distinctive UV–vis absorptions near 440 nm, irradiation into which brings about tautomerization to yield the divalent insertion product  $\text{HMNH}_2$ . This is not photostable but decomposes on exposure to broadband UV–visible light ( $\lambda = 200\text{--}800\text{ nm}$ ) giving place to the univalent species  $\text{MNH}_2$ . Additionally, the released H atoms react with  $\text{HMNH}_2$  to yield  $\text{H}_2\text{MNH}_2$ . Some of the results have been outlined in a preliminary communication.<sup>30</sup> The course of events as they occur in solid argon matrices at ca. 12 K has been tracked through the IR and UV–vis spectra of the matrices, and the identities of the products have been confirmed (i) by the response of the IR bands to isotopic enrichment in D or <sup>15</sup>N, (ii) by comparison with the results of density functional theory (DFT) calculations, and (iii) by reference to the properties of known cognate molecules. The properties observed or forecast for  $\text{M}\cdot\text{NH}_3$ ,  $\text{HMNH}_2$ ,  $\text{MNH}_2$ ,  $\text{H}_2\text{MNH}_2$ , and related molecules invite comparisons, particularly for the light they shed on the characters of the M–N bonds. The findings are analyzed too in relation to the experimental circumstances for insights into the mechanisms of the photochemical changes.

(11) Parnis, J. M.; Ozin, G. A. *J. Phys. Chem.* **1989**, 93, 1204–1215, 1220–1225.

(12) Xiao, Z. L.; Hauge, R. H.; Margrave, J. L. *Inorg. Chem.* **1993**, 32, 642–646.

(13) Lafleur, R. D.; Parnis, J. M. *J. Phys. Chem.* **1992**, 96, 2429–2433.

(14) Himmel, H.-J.; Downs, A. J.; Greene, T. M.; Andrews, L. *J. Chem. Soc., Chem. Commun.* **1999**, 2243–2244; *Organometallics* **2000**, 19, 1060–1070.

(15) Himmel, H.-J.; Downs, A. J.; Greene, T. M. *J. Am. Chem. Soc.* **2000**, 122, 922–930.

(16) Manceron, L., private communication.

(17) Himmel, H.-J.; Downs, A. J.; Greene, T. M., unpublished results.

(18) Howard, J. A.; Joly, H. A.; Edwards, P. P.; Singer, R. J.; Logan, D. E. *J. Am. Chem. Soc.* **1992**, 114, 474–477.

(19) Lanzisera, D. V.; Andrews, L. *J. Phys. Chem. A* **1997**, 101, 5082–5089.

(20) Meier, P. F.; Hauge, R. H.; Margrave, J. L. *J. Am. Chem. Soc.* **1978**, 100, 2108–2112.

(21) Kauffman, J. W.; Hauge, R. H.; Margrave, J. L. *High Temp. Sci.* **1984**, 17, 237–249. Szczepanski, J.; Szczesniak, M.; Vala, M. *Chem. Phys. Lett.* **1989**, 162, 123–126.

(22) Ball, D. W.; Hauge, R. H.; Margrave, J. L. *High Temp. Sci.* **1988**, 25, 95–101.

(23) Sakai, S. *J. Phys. Chem.* **1992**, 96, 8369–8373.

(24) Davy, R. D.; Jaffrey, K. L. *J. Phys. Chem.* **1994**, 98, 8930–8936.

(25) Marsh, C. M. B.; Hamilton, T. P.; Xie, Y.; Schaefer, H. F., III. *J. Chem. Phys.* **1992**, 96, 5310–5317.

(26) Hamilton, T. P.; Shaikh, A. W. *Inorg. Chem.* **1997**, 36, 754–755.

(27) Davy, R. D.; Schaefer, H. F., III. *Inorg. Chem.* **1998**, 37, 2291–2295.

(28) Fink, W. H.; Power, P. P.; Allen, T. L. *Inorg. Chem.* **1997**, 36, 1431–1436.

(29) Brothers, P. J.; Power, P. P. *Adv. Organomet. Chem.* **1996**, 39, 1–69. Power, P. P. *Chem. Rev.* **1999**, 99, 3463–3503.

(30) Himmel, H.-J.; Downs, A. J.; Greene, T. M. *J. Chem. Soc., Chem. Commun.* **2000**, 871–872.

## Experimental Section

Aluminum (Aldrich, purity 99.999%), gallium (Aldrich, purity 99.9999%), and indium (Aldrich, purity 99.999%) were each evaporated from a tantalum Knudsen cell that was heated resistively, to ca. 1000 °C for Al and 900 °C for Ga and In. Hence the metal vapor was co-deposited with an excess of NH<sub>3</sub>-doped argon on a CsI window cooled normally to ca. 12 K by means of a Displex closed-cycle refrigerator (Air Products model CS202). Fuller details of the matrix apparatus are given elsewhere.<sup>14</sup> The estimated proportions M:NH<sub>3</sub>:Ar (M = Al, Ga, or In) were typically in the order 1:2–12:600. Typical deposition rates were ca. 2 mmol of matrix gas per hour, continued over a period of 2–3 h. Similar experiments were carried out with ND<sub>3</sub> or <sup>15</sup>NH<sub>3</sub> in place of NH<sub>3</sub>. In some experiments too the argon matrix gas was doped not only with ammonia but also with up to 5% of H<sub>2</sub> or D<sub>2</sub>.

The following materials were used as received from the sources and with the stated purities listed: NH<sub>3</sub> (Aldrich, >99.99%), ND<sub>3</sub> (Aldrich, 99 at. % D), <sup>15</sup>NH<sub>3</sub> (Aldrich, 98 at. % <sup>15</sup>N), H<sub>2</sub> (BOC, Research grade), D<sub>2</sub> (Aldrich, 99.98 at. %), and argon (BOC, Research grade). Gas mixtures of argon with ammonia or with ammonia and dihydrogen were prepared by standard manometric methods.

Following deposition and IR or UV–vis analysis of the resulting matrix, the sample was exposed first to UV radiation with  $\lambda = 200$ –400 nm or to visible radiation with  $\lambda = \text{ca. } 436$  nm. Once the effects of such photolysis had been assessed, the sample was typically irradiated with broad-band UV–visible light with  $\lambda = 200$ –800 nm. The photolyzing radiation issuing from a Spectral Energy Hg–Xe arc lamp operating at 800 W was invariably limited by a water filter to absorb infrared radiation and so minimize any heating effects. UV light with  $\lambda = 200$ –400 nm was provided by the use of a visible block filter (Oriol). Visible radiation with  $\lambda = \text{ca. } 436$  nm and a band-pass of 20 nm was delivered via an appropriate interference filter (Oriol).

IR spectra of the matrix samples were recorded, typically at a resolution of 0.5 cm<sup>−1</sup> and with an accuracy of  $\pm 0.1$  cm<sup>−1</sup>, using a Nicolet Magna-IR 560 FTIR spectrometer equipped with a liquid N<sub>2</sub>-cooled MCTB or with a DTGS detector (for the ranges 4000–400 or 600–200 cm<sup>−1</sup>, respectively). UV–vis spectra were recorded in the range 300–900 nm using a Perkin-Elmer-Hitachi model 330 spectrophotometer.

Density functional theory (DFT) calculations were performed using the GAUSSIAN 98 program package<sup>31</sup> and applying the B3LYP method, which has been shown to give satisfactory results for small aluminum and gallium compounds.<sup>32</sup> A 6-311G(d) basis set was used for Al and Ga, a LANL2DZ basis set with additional d-polarization functions (exponent 0.5) for In.

## Results

The IR spectra associated with the products of the matrix reactions with ammonia will be reported in turn for aluminum, gallium, and indium atoms, respectively. Bands have been assigned on the basis of the following criteria: (i) their growth and decay characteristics in response to photolysis of the matrix under different conditions or to changes of reagent concentration; (ii) comparisons with the results of control experiments that did not include the metal atoms, or with the spectra of related species; (iii) consideration of the selection rules expected to govern the IR activity of a given molecule; (iv) the observed

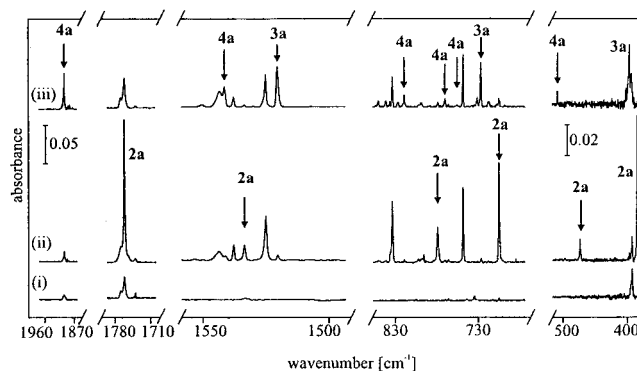


**Figure 1.** IR spectra of an Ar matrix containing Al and NH<sub>3</sub>: (i) following deposition, (ii) following UV photolysis ( $\lambda = 200$ –400 nm), and (iii) following broad-band UV–visible photolysis ( $\lambda = 200$ –800 nm).

effects of the naturally occurring <sup>69</sup>Ga and <sup>71</sup>Ga isotopes and of D- or <sup>15</sup>N-enrichment of the ammonia precursor; and (v) collation of the measured spectroscopic properties with those forecast by DFT calculations. Additionally, the UV–vis spectra of the matrices afforded a means of tracing the fate of the metal atoms through their interaction with ammonia molecules and the reactions subsequently induced by photolysis.

**Aluminum. (a) IR Spectra.** The spectrum recorded after deposition of Al together with 2% NH<sub>3</sub> in an argon matrix showed, besides the absorptions of NH<sub>3</sub> and [NH<sub>3</sub>]<sub>n</sub>,<sup>33</sup> three new absorptions at 3447.1, 1593.6, and 1131.4 cm<sup>−1</sup> due to a first reaction product **1a**. The only other features in the spectrum, invariably weak, were those associated with traces of impurity (H<sub>2</sub>O, [H<sub>2</sub>O]<sub>n</sub>, CO<sub>2</sub>, and CO)<sup>34</sup> that could be reduced to a minimum but never wholly eliminated. As reported previously,<sup>35</sup> the H<sub>2</sub>O gave rise to the insertion product HAlOH, which could be identified by its characteristic absorption at 1739.6 cm<sup>−1</sup>.

Upon photolysis at wavelengths near 436 nm or with UV light ( $\lambda = 200$ –400 nm) for a period of 5 min, the signals due to **1a** were extinguished and new signals at 3476.4, 1761.1, 1533.6, 778.7, 705.2, 483.8, 482.2, and 393.8 cm<sup>−1</sup> were observed to develop [see Figure 1(ii)]. According to their response to different photolysis times and to changes in the NH<sub>3</sub> or Al concentrations, these signals were judged to belong to a common absorber **2a**. The intense absorption at 1761.1 cm<sup>−1</sup> is close to the Al–H stretching frequencies observed in Al(II) species (e.g., AlH<sub>2</sub> 1806.3/1769.5,<sup>10</sup> HAlOH 1739.6,<sup>35</sup> CH<sub>3</sub>AlH 1764/1746 cm<sup>−1</sup><sup>11</sup>). In addition, the spectrum witnessed the appearance of three bands at 1525.1, 833.4, and 748.2 cm<sup>−1</sup>. These signals were found to decrease in experiments in which the concentration of NH<sub>3</sub> was reduced to 0.2%. The most likely explanation is that the signals belong to an ammonia adduct of **2a**.

After further photolysis, but with broad-band UV–visible radiation (200  $\leq \lambda \leq$  800 nm), the signals due to **2a** were found to decay with the simultaneous appearance and growth of a new family of bands located at 3495.1, 1520.3, 726.5, and 406.5 cm<sup>−1</sup> and belonging to a single carrier **3a** [see Figure 1(iii)]. Rather slower to develop but becoming increasingly conspicuous on continued photolysis was a second family of bands located at 3499.7, 1899.3, 1891.0, 1541.6, 818.7, 769.8, 755.0, 608.7, and 518.3 cm<sup>−1</sup> [see Figure 1(iii)], those at 1899.3, 818.7, 769.8,

(31) Frisch, M. J.; Trucks, G. W.; Schlegel, H. B.; Scuseria, G. E.; Robb, M. A.; Cheeseman, J. R.; Zakrzewski, V. G.; Montgomery, J. A., Jr.; Stratmann, R. E.; Burant, J. C.; Dapprich, S.; Millam, J. M.; Daniels, A. D.; Kudin, K. N.; Strain, M. C.; Farkas, O.; Tomasi, J.; Barone, V.; Cossi, M.; Cammi, R.; Mennucci, B.; Pomelli, C.; Adamo, C.; Clifford, S.; Ochterski, J.; Petersson, G. A.; Ayala, P. Y.; Cui, Q.; Morokuma, K.; Malick, D. K.; Rabuck, A. D.; Raghavachari, K.; Foresman, J. B.; Cioslowski, J.; Ortiz, J. V.; Stefanov, B. B.; Liu, G.; Liashenko, A.; Piskorz, P.; Komaromi, I.; Gomperts, R.; Martin, R. L.; Fox, D. J.; Keith, T.; Al-Laham, M. A.; Peng, C. Y.; Nanayakkara, A.; Gonzalez, C.; Challacombe, M.; Gill, P. M. W.; Johnson, B.; Chen, W.; Wong, M. W.; Andres, J. L.; Gonzalez, C.; Head-Gordon, M.; Replogle, E. S.; Pople, J. A. *GAUSSIAN 98*, Revision A.3; Gaussian Inc.: Pittsburgh, PA, 1998.

(32) Jursic, B. S. *J. Mol. Struct.: THEOCHEM* **1998**, 428, 61–66.

(33) See, for example: Süzer, S.; Andrews, L. *J. Chem. Phys.* **1987**, 87, 5131–5140. Abouaf-Marguin, L.; Jacox, M. E.; Milligan, D. E. *J. Mol. Spectrosc.* **1977**, 67, 34–61.

(34) Greene, T. M.; Andrews, L.; Downs, A. J. *J. Am. Chem. Soc.* **1995**, 117, 8180–8187.

(35) Hauge, R. H.; Kauffman, J. W.; Margrave, J. L. *J. Am. Chem. Soc.* **1980**, 102, 6005–6011.



**Table 1.** Infrared Absorptions (Frequencies in  $\text{cm}^{-1}$ ) Displayed by Ar Matrices Containing Al Atoms and  $^{14}\text{NH}_3/^{15}\text{NH}_3/^{14}\text{ND}_3$ 

Al + $^{14}\text{NH}_3$	Al + $^{15}\text{NH}_3$	Al + $^{14}\text{ND}_3$	deposition <sup>a</sup>	$\lambda = 436 \text{ nm}^a$	$\lambda = 200\text{--}800 \text{ nm}^a$	absorber
3499.7	<i>b</i>	<i>b</i>			↑	$\text{H}_2\text{AlNH}_2$ , <b>4a</b>
3495.1	3486.2	<i>b</i>			↑	$\text{AlNH}_2$ , <b>3a</b>
3476.4	3468.2	2595.6		↑	↓	$\text{HAlNH}_2$ , <b>2a</b>
3447.1	<i>b</i>	<i>b</i>	↑	↓		$\text{Al}\cdot\text{NH}_3$ , <b>1a</b>
1899.3	1899.3	1384.2			↑	$\text{H}_2\text{AlNH}_2$ , <b>4a</b>
1891.0	1891.0	<i>b</i>			↑	$\text{H}_2\text{AlNH}_2$ , <b>4a</b>
1887.6	1887.4	1364.7			↑	$\text{H}_2\text{AlNH}_2\cdot\text{NH}_3$
1761.1	1761.0	1282.6		↑	↓	$\text{HAlNH}_2$ , <b>2a</b>
1593.6	<i>b</i>	<i>b</i>	↑	↓		$\text{Al}\cdot\text{NH}_3$ , <b>1a</b>
1590.9	1590.9	<i>b</i>			↑	$\text{AlH}$
1541.6	1536.1	1159.5			↑	$\text{H}_2\text{AlNH}_2$ , <b>4a</b>
1533.6	1531.5	1151.4		↑	↓	$\text{HAlNH}_2$ , <b>2a</b>
1525.1	1520.0	1149.5		↑	↓	$\text{HAlNH}_2\cdot\text{NH}_3$
1520.3	1515.0	1137.8			↑	$\text{AlNH}_2$ , <b>3a</b>
1131.4	1125.6	972.6	↑	↓		$\text{Al}\cdot\text{NH}_3$ , <b>1a</b>
833.4	821.4	<i>b</i>		↑	↓	$\text{HAlNH}_2\cdot\text{NH}_3$
818.7	809.8	<i>b</i>			↑	$\text{H}_2\text{AlNH}_2$ , <b>4a</b>
778.7	766.9	748.3		↑	↓	$\text{HAlNH}_2$ , <b>2a</b>
769.8	766.2	611.0			↑	$\text{H}_2\text{AlNH}_2$ , <b>4a</b>
755.0	<i>b</i>	548.4			↑	$\text{H}_2\text{AlNH}_2$ , <b>4a</b>
748.2	<i>b</i>	<i>b</i>		↑		$\text{HAlNH}_2\cdot\text{NH}_3$
726.5	713.6	694.9			↑	$\text{AlNH}_2$ , <b>3a</b>
705.2	701.0	549.8		↑	↓	$\text{HAlNH}_2$ , <b>2a</b>
608.7	608.1	450.4			↑	$\text{H}_2\text{AlNH}_2$ , <b>4a</b>
518.3	516.7	397.7			↑	$\text{H}_2\text{AlNH}_2$ , <b>4a</b>
483.8	483.2	346.5		↑	↓	$\text{HAlNH}_2$ , <b>2a</b>
482.2	<i>b</i>	<i>b</i>		↑	↓	$\text{HAlNH}_2$ , <b>2a</b>
406.5	403.9	314.6			↑	$\text{AlNH}_2$ , <b>3a</b>
393.8	391.9	304.6		↑	↓	$\text{HAlNH}_2$ , <b>2a</b>

<sup>a</sup> ↑, increase; ↓, decrease. <sup>b</sup> Too weak to be detected or hidden by  $\text{NH}_3$  absorptions.

and  $608.7 \text{ cm}^{-1}$  being the most prominent. With constant relative intensities these arose from a common product **4a**. Diagnostic features of the spectrum are (i) the strong absorption at  $1899.3 \text{ cm}^{-1}$  occurring in the region characteristic of the stretching vibrations of terminal  $\text{Al(III)}\text{--H}$  bonds [cf.  $\text{AlH}_3$  ( $1882.9 \text{ cm}^{-1}$ ),<sup>10</sup>  $\text{HAlCl}_2$  ( $1967.6 \text{ cm}^{-1}$ ),<sup>36</sup> and  $[\text{H}_2\text{AlNMe}_2]_3$  ( $1800\text{--}1850 \text{ cm}^{-1}$ )<sup>37</sup>], (ii) the absorptions at  $3499.7$ ,  $1541.6$ , and  $608.7 \text{ cm}^{-1}$ , which are suggestive of the presence of an amido group,  $\text{NH}_2$ ,<sup>38</sup> and (iii) the appearance of an absorption at  $818.7 \text{ cm}^{-1}$ , which lies within the region expected for a  $\nu(\text{Al--N})$  mode of an aluminum(III) compound.<sup>19,39</sup> In addition to these signals, a very weak absorption at  $1887.6 \text{ cm}^{-1}$  was observed.

Experiments in which the matrix concentration of ammonia was reduced from 2 to 0.2%, while the other conditions remained as before, gave results identical to those described above, insofar as the intensities of the bands permitted them to be detected, but with one important difference: the yield of **4a** was reduced quite disproportionately—almost to vanishing point—in relation to those of **2a** and **3a**. In another series of experiments, the matrix was doped not only with 2%  $\text{NH}_3$  but also with up to 5%  $\text{H}_2$ . There was no sign of any reaction on deposition beyond the appearance of the IR bands associated with **1a**. UV photolysis ( $200 \leq \lambda \leq 400 \text{ nm}$ ) led as before to the formation of **2a** but now in company with  $\text{AlH}_2$  (recognizable by the appearance of prominent IR absorptions at  $1806.3$ ,  $1769.5$ , and  $766.4 \text{ cm}^{-1}$ ) as the principal photoproduct deriving from the reaction of photoexcited Al atoms with  $\text{H}_2$  under these conditions.<sup>10</sup> Irradiation with broad-band UV–visible light ( $200$

$\leq \lambda \leq 800 \text{ nm}$ ) then led to the formation of the products **3a** and **4a**, but now with a significantly *higher* yield of **4a** compared with **3a** than in comparable experiments with  $\text{H}_2$ -free matrices. The signal at  $1887.6 \text{ cm}^{-1}$  also gained in intensity. As expected,<sup>10</sup> there was a simultaneous decay of the bands due to  $\text{AlH}_2$ , these being replaced (i) by a single band at  $1649.1 \text{ cm}^{-1}$  and (ii) by a family of three bands at  $1882.9$ ,  $783.6$ , and  $697.7 \text{ cm}^{-1}$  readily identifiable with the molecules  $\text{AlH}$  and  $\text{AlH}_3$ , respectively.

The experiment was repeated successively with  $\text{ND}_3$  and  $^{15}\text{NH}_3$  with the results included in Table 1. The signal at  $1131.4 \text{ cm}^{-1}$  due to the species **1a** underwent a substantial shift in the experiment employing  $\text{ND}_3$  ( $\text{H/D} = 1.1633:1$ ) and a shift of  $-5.8 \text{ cm}^{-1}$  in that with  $^{15}\text{NH}_3$ .

The signals of product **2a** at  $3476.4$  and  $1533.6 \text{ cm}^{-1}$  exhibited H/D ratios of 1.3393:1 and 1.3319:1 and  $^{15}\text{N}$  shifts of  $-8.2$  and  $-2.1 \text{ cm}^{-1}$ , whereas the  $1761.1 \text{ cm}^{-1}$  signal showed an H/D ratio of 1.3731:1 and almost no  $^{15}\text{N}$  shift, in agreement with its assignment to an  $\text{Al--H}$  stretching fundamental. The bands at  $705.2$ ,  $483.8$ , and  $393.8 \text{ cm}^{-1}$  exhibited H/D ratios of 1.2826:1, 1.3962:1, and 1.2928:1 and  $^{15}\text{N}$  shifts of  $-4.2$ ,  $-0.6$  and  $-1.9 \text{ cm}^{-1}$ , respectively. No counterpart to the weak feature at  $482.2 \text{ cm}^{-1}$  could be discerned in the  $^{15}\text{NH}_3$  or  $\text{ND}_3$  experiments, being either too weak to be observed or hidden by other, stronger absorptions.

All four IR signals associated with the product **3a** could be traced to analogous features in the experiments with  $^{15}\text{NH}_3$  and  $\text{ND}_3$ . In keeping with its attribution to the scissoring fundamental of an  $\text{NH}_2$  fragment, the absorption at  $1520.3 \text{ cm}^{-1}$  exhibited an H/D ratio of 1.3362:1 and a  $^{15}\text{N}$  shift of  $-5.3 \text{ cm}^{-1}$ . The presence of an  $\text{NH}_2$  unit is also suggested by the band at  $3495.1 \text{ cm}^{-1}$  with a  $^{15}\text{N}$  shift of  $-8.9 \text{ cm}^{-1}$ . The bands at  $726.5$  and  $406.5 \text{ cm}^{-1}$  were characterized by H/D ratios of 1.0455:1 and 1.2921:1, and  $^{15}\text{N}$  shifts of  $-2.9$  and  $-2.6 \text{ cm}^{-1}$ , respectively.

(36) Schnöckel, H. J. *Mol. Struct.* **1978**, *50*, 275–280.

(37) Downs, A. J.; Duckworth, D.; Machell, J. C.; Pulham, C. R. *Polyhedron* **1992**, *11*, 1295–1304.

(38) Nakamoto, K. *Infrared and Raman Spectra of Inorganic and Coordination Compounds*, 5th ed.; Wiley-Interscience: New York, 1997; Part B. Lippert, M. F.; Power, P. P.; Sanger, A. R.; Srivastava, R. C. *Metal and Metalloid Amides*; Ellis Horwood: Chichester, U.K., 1980.

(39) Müller, J. J. *J. Am. Chem. Soc.* **1996**, *118*, 6370–6376.

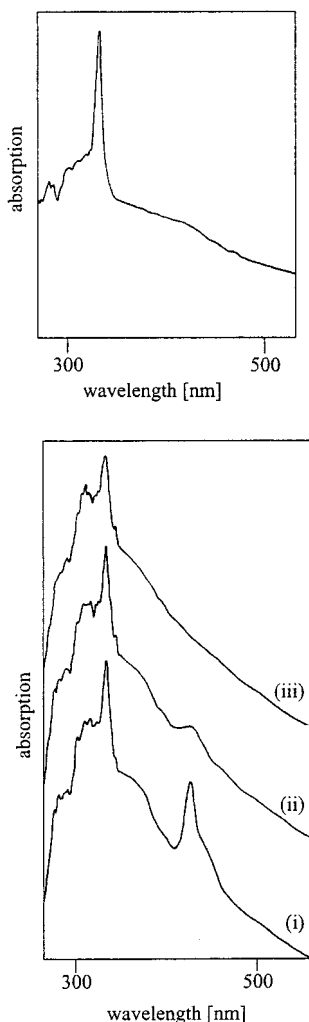


**Figure 2.** UV-vis spectra (a, top) of an Ar matrix containing Al, and (b, bottom) of an Ar matrix containing Al and  $\text{NH}_3$ : (i) following deposition, (ii) following photolysis with radiation having  $\lambda = 436$  nm, and (iii) following broad-band UV-visible photolysis ( $\lambda = 200$ –800 nm).

The strong band at  $1899.3\text{ cm}^{-1}$  of product **4a** exhibited a large frequency shift on deuteration ( $\text{H/D} = 1.3721:1$ ), but no significant  $^{15}\text{N}$  shift. Deuteration also elicited substantial shifts on the part of the bands at  $1541.6$  ( $\text{H/D} = 1.3295:1$ ),  $769.8$  ( $\text{H/D} = 1.3010:1$ ),  $755.0$  ( $1.3767:1$ ),  $608.7$  ( $1.3515:1$ ), and  $518.3\text{ cm}^{-1}$  ( $1.3032:1$ ), while  $^{15}\text{N}$  shifts amounting to  $-5.5$ ,  $-3.6$ ,  $-0.6$ , and  $-1.6\text{ cm}^{-1}$  were registered by the bands at  $1541.6$ ,  $769.8$ ,  $608.7$ , and  $518.3\text{ cm}^{-1}$ , respectively. The largest  $^{15}\text{N}$  shift ( $-8.9\text{ cm}^{-1}$ ) was associated with the feature at  $818.7\text{ cm}^{-1}$  for which it was unfortunately impossible to locate a counterpart in the  $\text{ND}_3$  experiments, presumably because of the masking effects of other absorptions.

**(b) UV-Vis Spectra.** Figure 2 depicts the UV-vis spectra measured over the range 300–900 nm for aluminum vapor isolated (a) in a pure argon matrix and (b) in an argon matrix doped with 2%  $\text{NH}_3$ . The first spectrum featured a strong absorption at 337 nm, which can be assigned on the basis of earlier studies<sup>40</sup> to the  $^2\text{S} \leftarrow ^2\text{P}$  transition of Al atoms. When the matrix included  $\text{NH}_3$ , this was accompanied by a new absorption at 428 nm. Irradiation of the  $\text{NH}_3$ -doped matrix for 5 min at wavelengths near 436 nm led to the disappearance of the new band. The IR spectrum measured at this stage witnessed

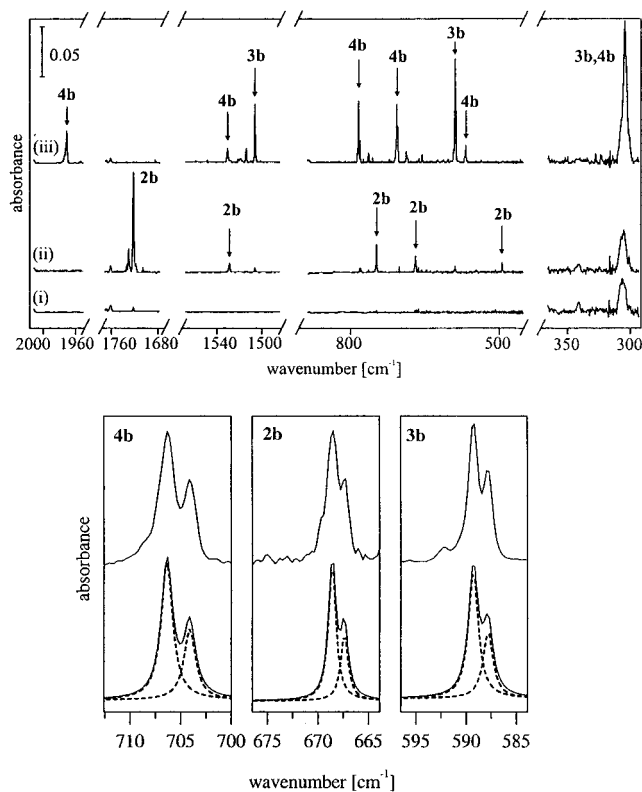


**Figure 3.** IR spectra of an Ar matrix containing Ga and  $\text{NH}_3$ : (a, top) (i) following deposition, (ii) following UV photolysis ( $\lambda = 200$ –400 nm), and (iii) following broad-band UV-visible photolysis ( $\lambda = 200$ –800 nm); (b, bottom) bands near 700 (**4b**), 670 (**2b**), and  $590\text{ cm}^{-1}$  (**3b**) showing  $^{69}\text{Ga}/^{71}\text{Ga}$  splitting.

the disappearance of the bands associated with **1a** as well as an increase of those due to the photoproduct **2a**.

**Gallium. (a) IR Spectra.** Figure 3 depicts the IR spectra displayed by an argon matrix containing ca. 0.2% Ga atoms and 2%  $\text{NH}_3$  before and after photolysis; details of the spectra are itemized in Table 2. On deposition, the matrix exhibited in addition to the absorptions characteristic of  $\text{NH}_3$  and  $[\text{NH}_3]_n$ <sup>33</sup> new features at  $3441.5$ ,  $1580.7$ , and  $1104.2\text{ cm}^{-1}$  carried by a common product **1b**. The only other features in the spectrum arose from traces of impurity ( $\text{H}_2\text{O}$ ,  $[\text{H}_2\text{O}]_n$ ,  $\text{CO}_2$ , and  $\text{CO}$ )<sup>34</sup> including the complex  $\text{Ga}\cdot\text{H}_2\text{O}$  identifiable by its characteristic absorption at  $1576.1\text{ cm}^{-1}$ .<sup>35</sup>

Exposure of the matrix to radiation at  $\lambda = \text{ca. } 436\text{ nm}$  or to UV radiation ( $\lambda = 200$ –400 nm) for 5 min brought about significant changes, as revealed by the IR spectrum measured at this stage [Figure 3a(ii)]. The bands due to **1b** had disappeared to be replaced by new ones at  $1721.8$ ,  $1528.7$ ,  $746.2$ ,  $668.5/667.4$ ,  $494.1$ , and  $210.9\text{ cm}^{-1}$  all attributable on the strength of their constant relative intensities to a second product **2b**. The most intense and distinctive features were those at  $1721.8$ ,  $668.5/667.4$ , and  $210.9\text{ cm}^{-1}$ , of which the first comes close in frequency to the Ga–H stretching fundamentals of the gallium-(II) species  $\text{GaH}_2$  ( $1799.5/1727.7\text{ cm}^{-1}$ ),<sup>10</sup>  $\text{CH}_3\text{GaH}$  ( $1719.7\text{ cm}^{-1}$ ),<sup>14</sup> and  $\text{HGaoH}$  ( $1669.8\text{ cm}^{-1}$ ).<sup>35</sup> The partially resolved doublet pattern at  $668.5/667.4\text{ cm}^{-1}$  revealed components with relative intensities of ca. 1.5:1 suggesting that it originates in a vibration involving appreciable motion of a single Ga atom ( $^{69}\text{Ga}$  and  $^{71}\text{Ga}$  in natural Ga being in the proportion 1.507:1<sup>41</sup>). Continued irradiation under these conditions produced little further change in the spectrum.

(40) Ammeter, J. H.; Schlosnagle, D. C. *J. Chem. Phys.* **1973**, *59*, 4784–4820.

(41) Lide, D. R., Editor-in-Chief. *CRC Handbook of Chemistry and Physics*, 80th ed.; CRC Press: Boca Raton, FL, 1999–2000.

**Table 2.** Infrared Absorptions (Frequencies in  $\text{cm}^{-1}$ ) Displayed by Ar Matrices Containing Ga Atoms and  $^{14}\text{NH}_3/^{15}\text{NH}_3/^{14}\text{ND}_3$ 

Ga + $^{14}\text{NH}_3$	Ga + $^{15}\text{NH}_3$	Ga + $^{14}\text{ND}_3$	deposition <sup>a</sup>	$\lambda = 436 \text{ nm}^a$	$\lambda = 200\text{--}800 \text{ nm}^a$	absorber
3510.7	3500.7	<i>b</i>			↑	$\text{H}_2\text{GaNH}_2$ , <b>4b</b>
<i>b</i>	3485.4	<i>b</i>		↑	↓	$\text{HGaNH}_2$ , <b>2b</b>
3471.6	<i>b</i>	<i>b</i>			↑	$\text{GaNH}_2$ , <b>3b</b>
3441.5	<i>b</i>	<i>b</i>	↑	↓		$\text{Ga}\cdot\text{NH}_3$ , <b>1b</b>
3413.4	3405.9	<i>b</i>			↑	$\text{H}_2\text{GaNH}_2$ , <b>4b</b>
1970.8 <sup>c</sup>	1970.7 <sup>c</sup>	1419.1			↑	$\text{H}_2\text{GaNH}_2$ , <b>4b</b>
1970.8 <sup>c</sup>	1970.7 <sup>c</sup>	1407.7			↑	$\text{H}_2\text{GaNH}_2$ , <b>4b</b>
1942.0	1942.0	<i>b</i>			↑	$\text{H}_2\text{GaNH}_2\cdot\text{NH}_3$
1721.8	1721.8	1249.5		↑	↓	$\text{HGaNH}_2$ , <b>2b</b>
1580.7	1576.9	<i>b</i>	↑	↓		$\text{Ga}\cdot\text{NH}_3$ , <b>1b</b>
1530.4	1524.3	1150.9			↑	$\text{H}_2\text{GaNH}_2$ , <b>4b</b>
1528.7	1523.2	1145.0		↑	↓	$\text{HGaNH}_2$ , <b>2b</b>
1513.8	1513.8	1090.1			↑	GaH
1505.9	1501.2	1132.6			↑	$\text{GaNH}_2$ , <b>3b</b>
1104.2	1099.1	824.9	↑	↓		$\text{Ga}\cdot\text{NH}_3$ , <b>1b</b>
782.8	778.3	605.1			↑	$\text{H}_2\text{GaNH}_2$ , <b>4b</b>
779.6	775.2	568.8			↑	$\text{H}_2\text{GaNH}_2$ , <b>4b</b>
754.3	751.0	<i>b</i>			↑	$\text{H}_2\text{GaNH}_2\cdot\text{NH}_3$
746.2	743.7	563.5		↑	↓	$\text{HGaNH}_2$ , <b>2b</b>
706.2/704.1	692.2/690.0	667.8/665.2			↑	$\text{H}_2\text{GaNH}_2$ , <b>4b</b>
668.5/667.4	652.8/651.4	626.8/625.1		↑	↓	$\text{HGaNH}_2$ , <b>2b</b>
589.3/587.9	574.3/573.1	557.9/556.4			↑	$\text{GaNH}_2$ , <b>3b</b>
567.7	567.4	405.9			↑	$\text{H}_2\text{GaNH}_2$ , <b>4b</b>
494.1	494.1	<i>b</i>		↑	↓	$\text{HGaNH}_2$ , <b>2b</b>
304.9	302.8	<i>b</i>			↑	$\text{H}_2\text{GaNH}_2$ , <b>4b</b>
303.3	302.7	<i>b</i>			↑	$\text{GaNH}_2$ , <b>3b</b>
210.9	<i>b</i>	<i>b</i>		↑	↓	$\text{HGaNH}_2$ , <b>2b</b>

<sup>a</sup> ↑, increase; ↓, decrease. <sup>b</sup> Too weak to be detected or hidden by  $\text{NH}_3$  absorptions. <sup>c</sup> Two modes contained within a single broad absorption.

By contrast, after photolysis for a further 30 min, but with broad-band UV–visible light ( $200 \leq \lambda \leq 800 \text{ nm}$ ), the matrix gave the IR spectrum illustrated in Figure 3a(iii). Hence it is apparent that the absorptions due to **2b** have decayed, while a new family of absorptions having a common origin in a third product **3b** has simultaneously appeared. These occurred at 3471.6, 1505.9, 589.3/587.9, and 303.3  $\text{cm}^{-1}$ , with the last two features being the most intense, and the doublet structure of the penultimate feature having all the hallmarks of  $^{69}\text{Ga}/^{71}\text{Ga}$  isotopic splitting. Extending the period of photolysis led to the buildup of **3b** at the expense of **2b**.

In addition to the bands due to **3b**, another family of bands, also with constant relative intensities and therefore originating in a fourth distinct product **4b**, was observed to develop [see Figure 3a(iii)], becoming increasingly prominent with photolysis times exceeding 30 min. The members of this family were located at 3510.7, 3413.4, 1970.8, 1530.4, 782.8, 779.6, 706.2/704.1, 567.7, and 304.9  $\text{cm}^{-1}$ , those at 1970.8, 782.8, 706.2/704.1, and 304.9  $\text{cm}^{-1}$  being the most intense (see Table 2). As in the case of the corresponding aluminum compound **4a**, there are several clues to the identity of **4b**: (i) the absorptions at 1970.8 and 779.6  $\text{cm}^{-1}$  are strongly suggestive of a terminal  $\text{GaH}_2$  unit in a trivalent gallane derivative [cf.  $\text{GaH}_3$  (1923.2 and 758.7  $\text{cm}^{-1}$ ),<sup>10</sup>  $\text{H}_2\text{GaCl}$  (1964.6/1978.1 and 731.4  $\text{cm}^{-1}$ ),<sup>42</sup>  $\text{H}_2\text{Ga}(\mu\text{-Cl})_2\text{GaH}_2$  (1994/2036 and 702/719  $\text{cm}^{-1}$ ),<sup>43</sup> and  $\text{H}_2\text{Ga}(\mu\text{-H})_2\text{BH}_2$  (1982/2005 and 729  $\text{cm}^{-1}$ )<sup>44</sup>]; (ii) the absorptions at 3510.7, 3413.4, 1530.4, 782.8, and 567.7  $\text{cm}^{-1}$  bear all the hallmarks of an  $\text{NH}_2$  group; and (iii) the doublet pattern at 706.2/704.1  $\text{cm}^{-1}$  implies  $^{69}\text{Ga}/^{71}\text{Ga}$  splitting arising from the motion of a single Ga atom, possibly in a  $\nu(\text{Ga-N})$  vibration. Once all signs of **2b** had disappeared, continued photolysis evoked little further change in the spectrum, **3b** and **4b** being

the ultimate photoproducts. In addition, the IR spectra contained very weak signals at 1942.0 and 754.3  $\text{cm}^{-1}$ , which developed simultaneously with those due to **4b**.

Experiments in which the matrix concentration of ammonia was reduced from 2 to 0.2%, while the other conditions remained as before, gave results identical to those described above, insofar as the intensities of the bands permitted them to be detected, but with one important difference: the yield of **4b** was reduced much more markedly than those of **2b** and **3b**.

In another series of experiments the matrix was doped not only with 2%  $\text{NH}_3$  but also with up to 5%  $\text{H}_2$ . The only signs of any reaction on deposition, beyond the appearance of the IR bands associated with **1b**, were those noted previously<sup>12,16</sup> and by us<sup>17</sup> for matrices formed by quenching Ga vapors with  $\text{H}_2$  and pointing to the spontaneous reaction of  $\text{Ga}_2$  dimers with  $\text{H}_2$  to give  $\text{Ga}(\mu\text{-H})_2\text{Ga}$ . UV photolysis led, as before, to the formation of **2b** but now in company with  $\text{GaH}_2$  (recognizable by the appearance of prominent IR absorptions at 1799.5, 1727.7, and 740.1  $\text{cm}^{-1}$ ) as the principal photoproduct deriving from the reaction of photoexcited Ga with  $\text{H}_2$  under these conditions.<sup>10,12</sup> Irradiation with broad-band UV–visible light then led to the formation of the products **3b** and **4b**, but now with a significantly *higher* yield of **4b** than in comparable experiments with  $\text{H}_2$ -free matrices. As expected, there was a simultaneous decay of the bands due to  $\text{GaH}_2$ , these being replaced by a single band at 1571.3  $\text{cm}^{-1}$  readily identifiable with the diatomic GaH molecule.<sup>10,12</sup>

To gain more information about the species **1b–4b**, the experiments were repeated using either  $\text{ND}_3$  or  $^{15}\text{NH}_3$  as the reagent, with the results included in Table 1. Hence it appeared that the perdeuterated version of the feature at 1104.2  $\text{cm}^{-1}$  due to **1b** was characterized by an IR band at 824.9  $\text{cm}^{-1}$ , whereas the  $^{15}\text{NH}_3$  version revealed a  $^{15}\text{N}$  shift of  $-5.1 \text{ cm}^{-1}$ . The signal at 1580.7  $\text{cm}^{-1}$  exhibited a  $^{15}\text{N}$  shift of  $-3.8 \text{ cm}^{-1}$ .

All the IR features of **2b** that could be observed with the switch from  $\text{NH}_3$  to  $\text{ND}_3$  appeared at lower frequency. Thus the bands at 1721.8, 1528.7, 746.2, and 668.5/667.4  $\text{cm}^{-1}$  for

(42) Köppe, R.; Schnöckel, H. *J. Chem. Soc., Dalton Trans.* **1992**, 3393–3395.

(43) Johnsen, E.; Downs, A. J.; Greene, T. M.; Souter, P. F.; Aarset, K.; Page, E. M.; Rice, D. A.; Richardson, A. N.; Brain, P. T.; Rankin, D. W. H.; Pulham, C. R. *Inorg. Chem.* **2000**, 39, 719–727.

(44) Pulham, C. R. D. Philos. Thesis, University of Oxford, U.K., 1991.

the natural isotopomer shifted to 1249.5 (H/D = 1.3780:1), 1145.0 (H/D = 1.3351:1), 563.5 (H/D = 1.3242:1), and 626.8/625.1 cm<sup>-1</sup> (H/D = 1.0665:1, 1.0677:1), respectively. No counterparts to the weak band at 494.1 cm<sup>-1</sup> and the stronger one at 210.9 cm<sup>-1</sup> could be observed for the perdeuterated version of **2b**, being either too weak to be detected or obscured by absorption from another source in the first case or outside the lower limit of detection (200 cm<sup>-1</sup>) in the second case. The IR spectrum of the <sup>15</sup>N isotopomer of **2b** resembled closely that of the natural form; while it lacked a band near 200 cm<sup>-1</sup> correlating with the lowest frequency transition of the latter, it included an additional band at 3485.4 cm<sup>-1</sup> strongly suggestive of a ν(N–H) mode. Of the bands in the spectrum of the natural isotopomer only those at 1528.7, 746.2, and 668.5/667.4 cm<sup>-1</sup> experienced significant frequency changes (–5.5, –2.5, and –15.7 to –16.0 cm<sup>-1</sup>, respectively) on <sup>15</sup>N substitution.

Three of the four absorptions associated with **3b** found parallels in the measured spectra of the perdeuterated and <sup>15</sup>N isotopomers. For example, those at 1505.9 and 589.3/587.9 cm<sup>-1</sup> moved to 1132.6 (H/D = 1.3296:1) and 557.9/556.4 cm<sup>-1</sup> (H/D = 1.0563:1, 1.0566:1), respectively, on deuteration, and showed <sup>14</sup>N/<sup>15</sup>N shifts (of –4.7 and –14.9 cm<sup>-1</sup>). No analogue of the weak band at 3471.6 cm<sup>-1</sup> associated with the isotopically normal form of **3b** could be discerned for either the deuterated or <sup>15</sup>N version, presumably for want of intensity and/or because of the masking effects of the more intense bands due to monomeric or oligomeric ammonia molecules.<sup>33</sup>

In its perdeuterated guise **4b** was characterized by eight detectable IR-active transitions. Hence the following shifts were observed: 1970.8 to 1419.1 cm<sup>-1</sup> (H/D = 1.3888:1), 1970.8 to 1407.7 cm<sup>-1</sup> (H/D = 1.4000:1), 1530.4 to 1150.9 cm<sup>-1</sup> (H/D = 1.3297:1), 782.8 to 605.1 cm<sup>-1</sup> (H/D = 1.2937:1), 779.6 to 568.8 cm<sup>-1</sup> (H/D = 1.3706:1), 706.2/704.1 to 667.8/665.2 cm<sup>-1</sup> (H/D = 1.058:1), and 567.7 to 405.9 cm<sup>-1</sup> (H/D = 1.3986:1). It was not possible to locate any bands in the spectrum of the deuterated compound corresponding to those at 3510.7, 3413.4, and 304.9 cm<sup>-1</sup> due to the isotopically natural species. <sup>15</sup>N substitution resulted in significant <sup>14</sup>N/<sup>15</sup>N shifts on the part of the features at the following frequencies (in cm<sup>-1</sup>): 3510.7 (–10.0), 3413.4 (–7.5), 1530.4 (–6.1), 782.8 (–4.5), 779.6 (–4.4), 706.2/704.1 (–14.0), and 304.9 (–2.1). By contrast, there was little or no change in the frequencies of the intense band at 1970.8 cm<sup>-1</sup> or the weaker one at 567.7 cm<sup>-1</sup>.

Experiments were also carried out with matrices containing Ga atoms and both NH<sub>3</sub> and D<sub>2</sub>. The presence of D<sub>2</sub> had no effect on the IR spectra characterizing the molecules **1b**, **2b**, and **3b**, which betrayed no sign of H/D exchange. On the other hand, the spectrum of **4b** was made distinctly more complicated, arguing for the presence of both Ga–H and Ga–D bonds in different H/D isotopomers of the molecule. As will be shown, these findings are highly germane in the mechanistic implications they carry.

**(b) UV–Vis Spectra.** Figure 4 shows typical UV–vis spectra measured over the range 300–900 nm for gallium vapor isolated (a) in a pure argon matrix and (b) in an argon matrix doped with 2% NH<sub>3</sub>. The furnace temperature for the evaporation of the gallium was set relatively low (ca. 900 °C) in this and all the other experiments so that Ga atoms should be the predominant metal species trapped in the matrices, with a negligible involvement of oligomers such as Ga<sub>2</sub>. Following deposition, the NH<sub>3</sub>-doped matrix was found to exhibit two prominent absorptions, one at 345 nm and the other at 440 nm. The former is recognizable on the basis of earlier studies<sup>13,14</sup> as the <sup>2</sup>S ←

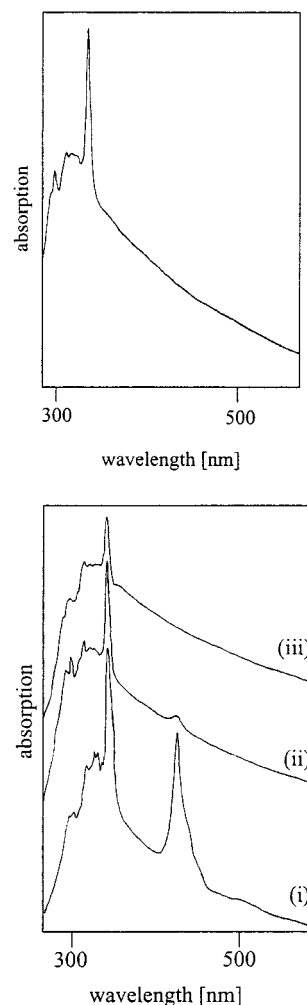


**Figure 4.** UV–vis spectra (a, top) of an Ar matrix containing Ga, and (b, bottom) of an Ar matrix containing Ga and NH<sub>3</sub>: (i) following deposition, (ii) following photolysis with radiation having  $\lambda = 436$  nm, and (iii) following broad-band UV–visible photolysis ( $\lambda = 200$ –800 nm).

<sup>2</sup>P transition of Ga atoms isolated in an argon matrix cage. The latter must then be associated with a relatively specific interaction between the Ga atoms and NH<sub>3</sub> dopant molecules, possibly corresponding to what is essentially a metal-based <sup>2</sup>S ← <sup>2</sup>P transition in a complex of the type Ga(NH<sub>3</sub>)<sub>n</sub>.

After 10 min irradiation with UV light ( $\lambda = 200$ –400 nm) or with visible light having  $\lambda =$  ca. 436 nm, it was found that the absorption at 440 nm had been virtually extinguished. The IR spectrum of the matrix measured at this stage witnessed the disappearance of the bands due to **1b** as well as the emergence of those due to the product **2b**. The UV absorption at 345 nm had also decayed somewhat but to a smaller extent. No new absorption could be detected either at this juncture or after exposure of the matrix to broad-band UV–visible radiation ( $\lambda = 200$ –800 nm), the only perceptible change in the UV–vis spectrum then being a further decrease in the intensity of the 345 nm signal. The IR measurements serve therefore to confirm that the initial appearance of the product **2b** is linked not only to the decay of the IR bands attributed to **1b** but also to that of the 440 nm band, providing strong circumstantial grounds for believing that **1b** is also the author of this latter feature.

**Indium. (a) IR Spectra.** Experiments with ammonia-doped argon matrices including indium in place of gallium followed



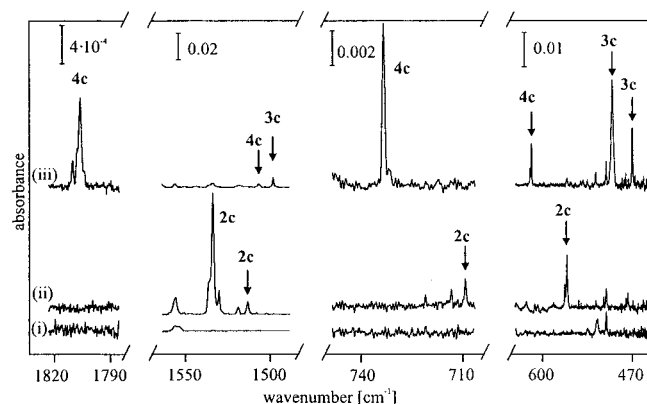


**Figure 5.** IR spectra of an Ar matrix containing In and  $\text{NH}_3$ : (i) following deposition, (ii) following UV photolysis ( $\lambda = 200\text{--}400\text{ nm}$ ), and (iii) following broad-band UV–visible photolysis ( $\lambda = 200\text{--}800\text{ nm}$ ).

the same pattern as those described above, and led to the identification of four products **1c**, **2c**, **3c**, and **4c** clearly analogous to the corresponding aluminum- and gallium-containing products **1a–4a** and **1b–4b**. A set of representative IR spectra measured for an argon matrix containing ca. 0.2% In atoms and 2%  $\text{NH}_3$  is reproduced in Figure 5; the relevant details of the spectra are listed in Table 3. Following deposition the spectrum [Figure 5(i)] witnessed the appearance of new absorptions at 3424.4 and 1082.9  $\text{cm}^{-1}$  requiring the conjunction of In and  $\text{NH}_3$  and attributable on the evidence of the earlier experiments to a complex **1c**, i.e., the In analogue of **1a** and **1b**. The only other features of the spectrum at this stage could be attributed to unchanged  $\text{NH}_3$  or  $[\text{NH}_3]_n$ <sup>33</sup> or to traces of the inevitable impurities, including  $\text{H}_2\text{O}$ ,  $[\text{H}_2\text{O}]_n$ , the adduct  $\text{In}\cdot\text{H}_2\text{O}$ ,  $\text{CO}_2$ , etc.<sup>34,35</sup>

Irradiation of the matrix at  $\lambda = \text{ca. } 436$  or  $200\text{--}400\text{ nm}$  for 5 min resulted in the decay of the absorptions due to **1c** and the growth of five new absorptions at 3463.5, 1533.8, 1512.9, 709.0, and 564.8  $\text{cm}^{-1}$  having but a single carrier, as indicated in Figure 5(ii). The most intense and distinctive feature was the one near 1530  $\text{cm}^{-1}$ , which occurs in the region where the In–H stretching mode of an indium(II) hydride might be expected (cf. 1615.6/1548.6, 1545.9, and 1486.5  $\text{cm}^{-1}$  for  $\text{InH}_2$ ,<sup>10</sup>  $\text{CH}_3\text{InH}$ ,<sup>14</sup> and  $\text{HInOH}$ ,<sup>35</sup> respectively). This factor, allied to the obvious affinities to the IR spectra of **2a** and **2b**, leads us to believe that the new bands are most plausibly ascribed to the indium analogue **2c**.

On the other hand, subsequent exposure of the matrix to broad-band UV–visible radiation ( $\lambda = 200\text{--}800\text{ nm}$ ) for 30 min brought about the decay of the bands due to **2c** with simultaneous growth of a new family of absorptions at 3481.7, 1498.1, 498.7, 469.6, and 237.0  $\text{cm}^{-1}$ . Given the circumstances of the experiment, the spectroscopic resemblance of this third product to **3a** and **3b** affords persuasive evidence that it is to be identified with the indium analogue **3c**. Moreover, weak features first detected at this stage and attributable to a fourth product were observed to grow on continued UV–visible photolysis. Most conspicuous of these was a band at 1805.9  $\text{cm}^{-1}$ , a frequency diagnostic of a  $\nu(\text{In–H})$  mode of an indium(III) hydride (cf. 1754.5, 1820.3/1804.0, and 1846.9  $\text{cm}^{-1}$  for  $\text{InH}_3$ ,<sup>10</sup>  $\text{H}_2\text{InCl}$ ,<sup>15</sup> and  $\text{HInCl}_2$ ,<sup>15</sup> respectively). Other, weaker features associated with this product occurred at 733.3 and 616.3  $\text{cm}^{-1}$ . All the signs are consistent therefore with the identification of the product with **4c**, the In counterpart to **4a** and **4b**.

The experiments giving rise to the species **1c–4c** were repeated using either  $\text{ND}_3$  or  $^{15}\text{NH}_3$  as the reagent, with the

results included in Table 3. Notable aspects of **1c** were the substantial deuterium shift ( $\text{H/D} = 1.3271:1$ ) and small  $^{15}\text{N}$  shift ( $-5.2\text{ cm}^{-1}$ ) of the band at 1082.9  $\text{cm}^{-1}$  as well as the  $^{15}\text{N}$  shift of  $-11.4\text{ cm}^{-1}$  for the band at 3424.4  $\text{cm}^{-1}$ . Four of the features associated with **2c** suffered deuterium shifts with H/D ratios ranging from 1.3833:1 (at 1533.8  $\text{cm}^{-1}$ ) to 1.0681:1 (at 564.8  $\text{cm}^{-1}$ ). The corresponding  $^{15}\text{N}$  shifts were 0 and  $-13.1\text{ cm}^{-1}$ . Experiments with  $\text{ND}_3$  yielded two absorptions identifiable with perdeuterated **3c** (at 1116.3 and 480.6  $\text{cm}^{-1}$ ) appearing to correlate with the absorptions at 1498.1 and 498.7  $\text{cm}^{-1}$  in the spectrum of the normal isotopomer. The H/D ratios were therefore 1.3420:1 and 1.0377:1, respectively. Three features could be definitely traced to the  $^{15}\text{N}$  isotopomer indicating  $^{15}\text{N}$  shifts amounting to  $-4.5$ ,  $-10.5$ , and  $-1.6\text{ cm}^{-1}$  for the transitions occurring at 1498.1, 498.7, and 237.0  $\text{cm}^{-1}$ , respectively.

Weakness and the potential for masking by the signals due to other, more abundant molecules ( $\text{NH}_3$ ,  $[\text{NH}_3]_n$ , **3c**, etc.) meant that there was only limited access to the IR-active transitions carried by **4c** in its normal, deuterated, or  $^{15}\text{N}$  versions. However, decreasing the  $\text{NH}_3$  concentration did appear to reduce the yield of **4c** significantly more than that of **3c**, whereas adding  $\text{H}_2$  to the matrix boosted the proportion of **4c** relative to **3c**. It was also possible to establish that the 1805.9  $\text{cm}^{-1}$  transition moved to 1299.0  $\text{cm}^{-1}$  on deuteration of **4c** giving  $\text{H/D} = 1.3902:1$  but was unmoved when  $^{14}\text{N}$  was replaced by  $^{15}\text{N}$ . On the other hand, the bands at 733.3 and 616.3  $\text{cm}^{-1}$  displayed  $^{15}\text{N}$  shifts of  $-1.9$  and  $-17.1\text{ cm}^{-1}$ , respectively. With  $\text{ND}_3$  as the reagent, a weak band was observed at 474.6  $\text{cm}^{-1}$ ; this showed the growth pattern characteristic of the IR features belonging to **4c** but could not be traced to any obvious counterparts in the spectra of the normal and  $^{15}\text{N}$  versions of the molecule. The yield of **4c** was invariably small; in no case did it match those of its aluminum and gallium analogues. This may reflect significant photolability on its part or lower yields of the intermediates leading to its formation. Although spectroscopic details about **4c** are therefore rather sparse, all the features that could be observed are consistent with the circumstantial evidence pointing to a product akin to **4a** and **4b**.

**(b) UV–Vis Spectra.** UV–vis spectra of indium vapor entrapped (a) in a pure argon matrix and (b) in an argon matrix doped with 2%  $\text{NH}_3$  are depicted in Figure 6. Both spectra include a prominent absorption at 335 nm attributable to the  $^2\text{S} \leftarrow ^2\text{P}$  transition of In atoms trapped in an argon matrix cage.<sup>14,45</sup> The presence of  $\text{NH}_3$  gave rise, however, to a new intense absorption centered at 435 nm. Irradiation of the matrix with visible light having  $\lambda = 436\text{ nm}$  for 10 min virtually extinguished this second feature. At the same time the IR spectra bore witness to the disappearance of the bands characteristic of **1c** and to the appearance of those characteristic of **2c**. Accordingly we are led to conclude that the visible absorption at 435 nm belongs to **1c** and that irradiation into it offers a highly efficient means of converting **1c** into **2c**. Further photolysis with either broad-band UV or UV–visible light resulted in no change in the UV–vis spectrum of the  $\text{NH}_3$ -doped matrix beyond the gradual decay of the 335 nm absorption.

## Discussion

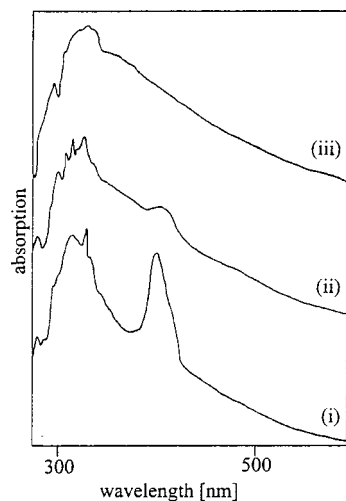
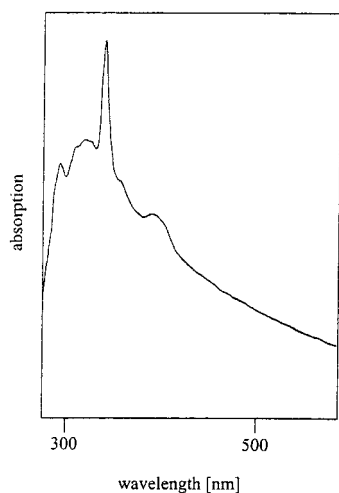
The main IR features observed to develop as the result of the reactions induced thermally or photolytically on deposition of Al, Ga, or In atoms in an ammonia-doped argon matrix will

(45) Schroeder, W.; Rotermund, H.-H.; Wiggenshauser, H.; Schrittenlacher, W.; Hormes, J.; Krebs, W.; Laaser, W. *Chem. Phys.* **1986**, *104*, 435–448.

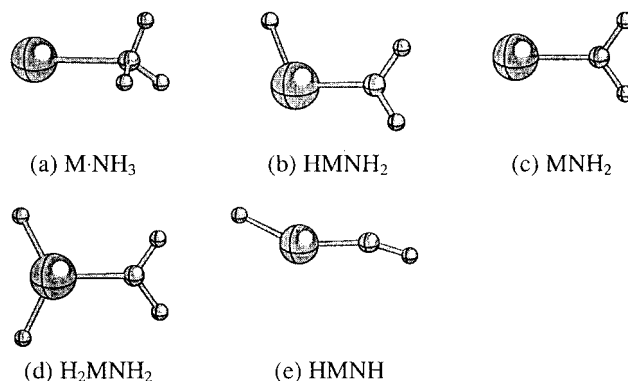
**Table 3.** Infrared Absorptions (Frequencies in cm<sup>-1</sup>) Displayed by Ar Matrices Containing In Atoms and <sup>14</sup>NH<sub>3</sub>/<sup>15</sup>NH<sub>3</sub>/<sup>14</sup>ND<sub>3</sub>

In + <sup>14</sup> NH <sub>3</sub>	In + <sup>15</sup> NH <sub>3</sub>	In + <sup>14</sup> ND <sub>3</sub>	deposition <sup>a</sup>	λ = 436 nm <sup>a</sup>	λ = 200–800 nm <sup>a</sup>	absorber
3481.7	<i>b</i>	<i>b</i>			↑	InNH <sub>2</sub> , <b>3c</b>
3463.5	<i>b</i>	<i>b</i>		↑	↓	HInNH <sub>2</sub> , <b>2c</b>
3424.4	3413.0	<i>b</i>	↑	↓		In·NH <sub>3</sub> , <b>1c</b>
1805.9	1805.9	1299.0			↑	H <sub>2</sub> InNH <sub>2</sub> , <b>4c</b>
1533.8	1533.8	1108.8		↑	↓	HInNH <sub>2</sub> , <b>2c</b>
1512.9	<i>b</i>	1122.2		↑	↓	HInNH <sub>2</sub> , <b>2c</b>
1506.6	<i>b</i>	<i>b</i>			↑	H <sub>2</sub> InNH <sub>2</sub> , <b>4c</b>
1498.1	1493.6	1116.3			↑	InNH <sub>2</sub> , <b>3c</b>
1387.3	1387.3	995.8			↑	InH
1082.9	1077.7	816.0	↑	↓		In·NH <sub>3</sub> , <b>1c</b>
733.3	731.4	<i>b</i>			↑	H <sub>2</sub> InNH <sub>2</sub> , <b>4c</b>
713.3	<i>b</i>	<i>b</i>		↑	↓	HInOH
709.0	<i>b</i>	522.9		↑	↓	HInNH <sub>2</sub> , <b>2c</b>
616.3	599.2	<i>b</i>			↑	H <sub>2</sub> InNH <sub>2</sub> , <b>4c</b>
564.8	551.7	528.8		↑	↓	HInNH <sub>2</sub> , <b>2c</b>
522.6	522.6	505.3			↑	InOH
498.7	488.2	480.6			↑	InNH <sub>2</sub> , <b>3c</b>
<i>b</i>	<i>b</i>	474.6			↑	H <sub>2</sub> InNH <sub>2</sub> , <b>4c</b>
469.6	<i>b</i>	<i>b</i>			↑	InNH <sub>2</sub> , <b>3c</b>
237.0	235.4	<i>b</i>			↑	InNH <sub>2</sub> , <b>3c</b>

<sup>a</sup> ↑, increase; ↓, decrease. <sup>b</sup> Too weak to be detected or hidden by NH<sub>3</sub> absorptions.

**Figure 6.** UV–vis spectra (a, top) of an Ar matrix containing In, and (b, bottom) of an Ar matrix containing In and NH<sub>3</sub>: (i) following deposition, (ii) following photolysis with radiation having λ = 436 nm, and (iii) following broad-band UV–visible photolysis (λ = 200–800 nm).

be shown to arise from the four products M·NH<sub>3</sub> (**1a–1c**), HMNH<sub>2</sub> (**2a–2c**), MNH<sub>2</sub> (**3a–3c**), and H<sub>2</sub>MNH<sub>2</sub> (**4a–4c**), where M = Al, Ga, or In. Few of these monomeric molecules

**Figure 7.** Calculated geometries of the molecules (a) M·NH<sub>3</sub>, (b) HMNH<sub>2</sub>, (c) MNH<sub>2</sub>, (d) H<sub>2</sub>MNH<sub>2</sub>, and (e) HMNH (M = Al, Ga, or In).

have been described previously in more than hypothetical terms, although amidogallane is familiar experimentally in its trimeric form, [H<sub>2</sub>GaNH<sub>2</sub>]<sub>3</sub>, which is stable at temperatures up to nearly 150 °C.<sup>3</sup> The assignments will be justified by consideration of the frequencies and isotopic shifts of the observed bands and by comparisons either with the vibrational properties of the molecules anticipated by DFT calculations or with the vibrational properties reported for related species.

**M·NH<sub>3</sub> [M = Al (**1a**), Ga (**1b**), or In (**1c**)].** The observed IR signatures of each of the products **1a**, **1b**, and **1c**, formed on co-deposition of the metal atoms with ammonia, are wholly consistent with the presence of one or more NH<sub>3</sub> molecules perturbed by interaction with the metal. The conditions of the experiments were deliberately engineered to ensure that the matrices contained M atoms to the virtual exclusion of oligomers M<sub>n</sub>.<sup>14</sup> Accordingly it seems unlikely that **1a**, **1b**, or **1c** contains more than one M atom. That the intensities of both the IR and visible absorptions should vary roughly in *direct* proportion to the matrix concentration of ammonia argues strongly, moreover, for the formulation of each of these species as M·NH<sub>3</sub>.

DFT calculations find a global minimum for the ground state of such a molecule with the geometry represented in Figure 7a; the optimized dimensions and vibrational properties are given in Table 4. As expected, each of the molecules resembles Al·NH<sub>3</sub><sup>23,24</sup> in deviating slightly from regular C<sub>3v</sub> symmetry;

**Table 4.** Comparison between the IR Spectra Observed and Calculated (Frequencies in  $\text{cm}^{-1}$ ) for  $\text{M}\cdot^{14}\text{NH}_3/\text{M}\cdot^{15}\text{NH}_3/\text{M}\cdot^{14}\text{ND}_3$  (**1a–1c**) ( $\text{M} = \text{Al, Ga, or In}$ )

$\text{M}\cdot^{14}\text{NH}_3$		$\text{M}\cdot^{15}\text{NH}_3$		$\text{M}\cdot^{14}\text{ND}_3$		assignment	description of vibrational mode	M
obsd	calcd <sup>a</sup>	obsd	calcd <sup>a</sup>	obsd	calcd <sup>a</sup>			
3447.1	3573.1 (43)	<i>b</i>	3563.1 (43)	<i>b</i>	2632.9 (22)	$\nu_1$ (a')	$\nu_{\text{asym}}(\text{N-H})$	Al
<i>b</i>	3458.2 (3)	<i>b</i>	3456.0 (2)	<i>b</i>	2470.1 (4)	$\nu_2$ (a')	$\nu_{\text{sym}}(\text{N-H})$	
<i>b</i>	1722.4 (31)	<i>b</i>	1719.2 (32)	<i>b</i>	1247.9 (13)	$\nu_3$ (a')	$\delta_{\text{asym}}(\text{NH}_3)$	
1131.4	1231.0 (174)	1125.6	1224.5 (170)	972.6	936.3 (122)	$\nu_4$ (a')	$\delta_{\text{sym}}(\text{NH}_3)$	
<i>b</i>	429.9 (8)	<i>b</i>	428.5 (8)	<i>b</i>	318.7 (4)	$\nu_5$ (a')	$\rho(\text{NH}_3)$	
<i>b</i>	244.8 (27)	<i>b</i>	240.7 (26)	<i>b</i>	232.8 (23)	$\nu_6$ (a')	$\nu(\text{Al-N})$	
<i>b</i>	3544.0 (5)	<i>b</i>	3535.2 (5)	<i>b</i>	2599.7 (2)	$\nu_7$ (a'')	$\nu_{\text{asym}}(\text{N-H})$	
1593.6	1600.1 (20)	<i>b</i>	1597.5 (20)	<i>b</i>	1156.4 (8)	$\nu_8$ (a'')	$\delta_{\text{asym}}(\text{NH}_3)$	
<i>b</i>	250.5 (1)	<i>b</i>	249.6 (1)	<i>b</i>	187.0 (0)	$\nu_9$ (a'')	$\rho(\text{NH}_3)$	
3441.5	3594.3 (29)	<i>b</i>	3584.3 (29)	<i>b</i>	2648.0 (16)	$\nu_1$ (a')	$\nu_{\text{asym}}(\text{N-H})$	Ga
<i>b</i>	3473.6 (5)	<i>b</i>	3471.4 (5)	<i>b</i>	2480.7 (6)	$\nu_2$ (a')	$\nu_{\text{sym}}(\text{N-H})$	
<i>b</i>	1728.9 (30)	<i>b</i>	1725.7 (30)	<i>b</i>	1253.6 (14)	$\nu_3$ (a')	$\delta_{\text{asym}}(\text{NH}_3)$	
1104.2	1189.4 (153)	1099.1	1183.1 (150)	824.9	906.1 (107)	$\nu_4$ (a')	$\delta_{\text{sym}}(\text{NH}_3)$	
<i>b</i>	368.0 (15)	<i>b</i>	366.9 (15)	<i>b</i>	271.6 (6)	$\nu_5$ (a')	$\rho(\text{NH}_3)$	
<i>b</i>	204.7 (17)	<i>b</i>	200.1 (17)	<i>b</i>	191.4 (14)	$\nu_6$ (a')	$\nu(\text{Ga-N})$	
<i>b</i>	3565.5 (2)	<i>b</i>	3556.5 (2)	<i>b</i>	2617.0 (1)	$\nu_7$ (a'')	$\nu_{\text{asym}}(\text{N-H})$	
1580.7	1590.6 (12)	1576.9	1587.8 (13)	<i>b</i>	1151.2 (5)	$\nu_8$ (a'')	$\delta_{\text{asym}}(\text{NH}_3)$	
<i>b</i>	279.7 (9)	<i>b</i>	278.7 (9)	<i>b</i>	207.4 (3)	$\nu_9$ (a'')	$\rho(\text{NH}_3)$	
3424.4	3542.3 (24)	3413.0	3532.7 (24)	<i>b</i>	2593.9 (14)	$\nu_1$ (a')	$\nu_{\text{asym}}(\text{N-H})$	In
<i>b</i>	3414.7 (4)	<i>b</i>	3412.4 (3)	<i>b</i>	2437.2 (5)	$\nu_2$ (a')	$\nu_{\text{sym}}(\text{N-H})$	
<i>b</i>	1683.8 (30)	<i>b</i>	1680.7 (30)	<i>b</i>	1217.1 (15)	$\nu_3$ (a')	$\delta_{\text{asym}}(\text{NH}_3)$	
1082.9	1171.7 (133)	1077.7	1165.4 (130)	816.0	884.5 (90)	$\nu_4$ (a')	$\delta_{\text{sym}}(\text{NH}_3)$	
<i>b</i>	291.2 (26)	<i>b</i>	290.2 (26)	<i>b</i>	214.0 (11)	$\nu_5$ (a')	$\rho(\text{NH}_3)$	
<i>b</i>	157.8 (16)	<i>b</i>	154.0 (15)	<i>b</i>	143.6 (13)	$\nu_6$ (a')	$\nu(\text{In-N})$	
<i>b</i>	3521.5 (6)	<i>b</i>	3512.7 (6)	<i>b</i>	2571.9 (3)	$\nu_7$ (a'')	$\nu_{\text{asym}}(\text{N-H})$	
<i>b</i>	1451.0 (4)	<i>b</i>	1448.6 (4)	<i>b</i>	1046.4 (2)	$\nu_8$ (a'')	$\delta_{\text{asym}}(\text{NH}_3)$	
<i>b</i>	252.4 (13)	<i>b</i>	251.6 (13)	<i>b</i>	185.5 (5)	$\nu_9$ (a'')	$\rho(\text{NH}_3)$	

<sup>a</sup>  $\text{Al}\cdot\text{NH}_3$  symmetry  $C_s$ :  $\text{Al-N}$  2.3344 Å,  $\text{N-H}(1)$  1.0162 Å,  $\text{N-H}(2,3)$  1.0168 Å,  $\text{Al-N-H}(1)$  114.2°,  $\text{Al-N-H}(2,3)$  109.9°.  $\text{Ga}\cdot\text{NH}_3$  symmetry  $C_s$ :  $\text{Ga-N}$  2.4560 Å,  $\text{N-H}(1)$  1.0148 Å,  $\text{N-H}(2,3)$  1.0157 Å,  $\text{Ga-N-H}(1)$  113.9°,  $\text{Ga-N-H}(2,3)$  109.9°.  $\text{In}\cdot\text{NH}_3$  symmetry  $C_s$ :  $\text{In-N}$  2.7084 Å,  $\text{N-H}(1)$  1.0244 Å,  $\text{N-H}(2,3)$  1.0252 Å,  $\text{In-N-H}(1)$  114.3°,  $\text{In-N-H}(2,3)$  111.2°. Intensities ( $\text{km mol}^{-1}$ ) are given in parentheses. <sup>b</sup> Too weak to be detected or hidden by ammonia absorptions or out of range of detection.

this is achieved through one N–H bond being slightly shorter than the other two and the H–N–H angles being fractionally different so that the overall symmetry is  $C_s$  and there are as a result not 6 but 9 distinct vibrational fundamentals. At 2.3344, 2.4560, and 2.7084 Å, the calculated  $\text{M}\cdots\text{N}$  distances in  $\text{Al}\cdot\text{NH}_3$ ,  $\text{Ga}\cdot\text{NH}_3$ , and  $\text{In}\cdot\text{NH}_3$ , respectively, come as something of a surprise, being about 1 Å shorter than the sum of the relevant van der Waals radii and implying a far from insignificant interaction between the two centers.

Comparisons between the IR spectra observed and those predicted are limited by the weakness of many of the transitions in IR absorption and by the masking effects of ammonia or water bands. Nevertheless, the features that could be detected for each complex were in satisfactory agreement with the properties forecast by the DFT calculations. Identifiable with the symmetric  $\text{NH}_3$  deformation,  $\nu_2$  ( $a_1$ ), is the band at 1131.4  $\text{cm}^{-1}$  for **1a**, at 1104.2  $\text{cm}^{-1}$ , for **1b** and at 1082.9  $\text{cm}^{-1}$  for **1c**. These assignments are supported by the responses to isotopic change. With respect to  $\nu_2$  of matrix-isolated  $\text{NH}_3$  at 974.5  $\text{cm}^{-1}$ , therefore, we find blue shifts of 156.9, 129.7 and 108.4  $\text{cm}^{-1}$  for **1a**, **1b**, and **1c**, respectively. Similar in sense but smaller in magnitude, these features show parallels with the vibrational properties of  $\text{NH}_3$  molecules coordinated to metal cations<sup>38</sup> and therefore imply  $\text{M}\cdots\text{N}$  interaction between the metal and ammonia molecules in **1a**, **1b**, and **1c**. Hence the ammonia adducts of Al, Ga, and In exhibit a  $\delta_{\text{sym}}(\text{NH}_3)$  mode with a blue shift similar to those observed previously<sup>47</sup> for the alkali metal adducts  $\text{Li}\cdot\text{NH}_3$ ,  $\text{Na}\cdot\text{NH}_3$ ,  $\text{K}\cdot\text{NH}_3$ , and  $\text{Cs}\cdot\text{NH}_3$ . The bands at 3447.1  $\text{cm}^{-1}$  for **1a**, at 3441.5  $\text{cm}^{-1}$  for **1b**, and at 3424.4  $\text{cm}^{-1}$  for **1c** are identifiable with the antisymmetric N–H stretching fundamental,  $\nu_1$  (a'). The  $^{15}\text{N}$  shift of  $-11.4 \text{ cm}^{-1}$  observed for **1c** confirms this assignment. Thus, the frequencies are close to

that of the corresponding  $\nu_3$  (e) fundamental of uncoordinated  $\text{NH}_3$  (3434.0  $\text{cm}^{-1}$ ).<sup>33</sup> This observation is in general agreement with the results of our DFT calculations [3585.3  $\text{cm}^{-1}$  for  $\nu_3$  (e) in  $\text{NH}_3$ ; 3573.1, 3594.3, and 3542.3  $\text{cm}^{-1}$  for  $\nu_1$  (a') in  $\text{Al}\cdot\text{NH}_3$ ,  $\text{Ga}\cdot\text{NH}_3$ , and  $\text{In}\cdot\text{NH}_3$ , respectively]. In the case of the alkali metals, the symmetric N–H stretching mode was observed to be the most intense feature in the spectra of the adducts. For the group 13 metal adducts, however, the calculations indicate that  $\nu_{\text{asym}}(\text{N-H})$  gives the most intense IR absorption in this region. We have also calculated the IR spectrum of  $\text{Li}\cdot\text{NH}_3$  ( $C_{3v}$  symmetry;  $\text{Li-N}$  1.9933,  $\text{N-H}$  1.0210 Å;  $\text{H-N-H}$  106.7°), with the following results (frequencies in  $\text{cm}^{-1}$ , intensities in  $\text{km mol}^{-1}$  in brackets):  $\nu_{\text{asym}}(\text{N-H})$   $\text{NH}_3$  3585.3 (3),  $\text{Li}\cdot\text{NH}_3$  3496.6 (64);  $\nu_{\text{sym}}(\text{N-H})$   $\text{NH}_3$  3464.2 (1),  $\text{Li}\cdot\text{NH}_3$  3381.1 (586);  $\delta_{\text{sym}}(\text{NH}_3)$   $\text{NH}_3$  1122.7 (202),  $\text{Li}\cdot\text{NH}_3$  1252.0 (105.7). The large increase in intensity of the absorptions of ammonia brought about by coordination has been previously correlated with the degree of metal-to-ligand charge transfer in the adduct.<sup>46</sup> On the basis of this correlation, the degree of charge transfer appears, as expected, to be considerably higher in the alkali metal adducts than in the group 13 metal adducts.

The third absorption present in the spectra of **1a** and **1b** (at 1593.6 and 1580.7  $\text{cm}^{-1}$ ) is identifiable with the  $\delta_{\text{asym}}(\text{NH}_3)$  mode of  $\text{Al}\cdot\text{NH}_3$  and  $\text{Ga}\cdot\text{NH}_3$ , respectively. It was not possible unfortunately to locate a transition corresponding to the  $\nu(\text{M-N})$  fundamental, which is not expected to be very intense in IR absorption and, with a predicted frequency of 244.8, 204.7, or 157.8  $\text{cm}^{-1}$  for Al, Ga, or In, respectively, is likely to fall below the low-frequency threshold of detection (200  $\text{cm}^{-1}$ ) in our experiments.



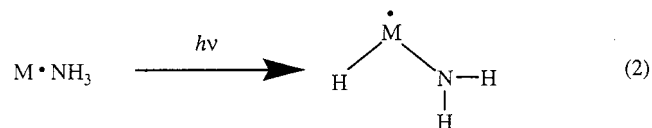
We have investigated possible excited states of Ga·NH<sub>3</sub> in order to determine the likely origin and photochemical role of the electronic transition near 440 nm. On the evidence available, we believe this and the related features of Al·NH<sub>3</sub> and In·NH<sub>3</sub> to be essentially a metal-based <sup>2</sup>S ← <sup>2</sup>P transition appreciably red-shifted by the coordinating action of the NH<sub>3</sub> molecule. The reaction energies for the formation of the adducts starting from the metal atom in its <sup>2</sup>P ground state and NH<sub>3</sub> were found to be −60.2, −51.8, and −28.8 kJ mol<sup>−1</sup> for M = Al, Ga, and In, respectively.

**HMNH<sub>2</sub> [M = Al (2a), Ga (2b), or In (2c)].** As noted previously, the IR bands at 1761.1, 1721.8, and 1533.8 cm<sup>−1</sup> are highly suggestive of a ν(M–H) fundamental of **2a** (M = Al), **2b** (M = Ga), and **2b** (M = In), respectively, where M is in a divalent state. The observed H/D ratios of 1.3731 for **2a**, 1.3780:1 for **2b**, and 1.3833:1 for **2c** are in keeping with those for other monohydrides, e.g., CH<sub>3</sub>GaH 1.3827:1,<sup>14</sup> CH<sub>3</sub>InH 1.3864:1,<sup>14</sup> HFeNH<sub>2</sub> 1.3890:1,<sup>21</sup> and HNiNH<sub>2</sub> 1.3401:1.<sup>22</sup> The aluminum compound HAlNH<sub>2</sub> has been reported previously, having been identified by its IR spectrum in argon matrices containing laser-ablated Al atoms and NH<sub>3</sub>;<sup>19</sup> the results presented here generally tally with, but are more extensive than, those of the earlier study.

The absorption at 1533.6 cm<sup>−1</sup> (H/D ratio 1.3319:1) is characteristic of an NH<sub>2</sub> scissoring mode of **2a**,<sup>38</sup> thus pointing to the presence of an NH<sub>2</sub> fragment. What appears to be the ν<sub>sym</sub>(N–H) mode of the NH<sub>2</sub> group, located at 3476.4 cm<sup>−1</sup> (H/D ratio 1.3393:1), was also detected. Support for these assignments comes from the <sup>14</sup>N/<sup>15</sup>N shifts of the two bands (−2.1 and −8.2 cm<sup>−1</sup>, respectively). Next in order of decreasing frequency comes the signal at 778.7 cm<sup>−1</sup>, which can be assigned to the ν(Al–N) fundamental on the basis of its H/D ratio (1.0406:1) and its <sup>15</sup>N shift (−11.8 cm<sup>−1</sup>). The observation of these bands gives strong grounds for believing that **2a** is HAlNH<sub>2</sub>. The signal at 705.2 cm<sup>−1</sup> (H/D ratio 1.2826, <sup>15</sup>N shift −4.2 cm<sup>−1</sup>) is then attributable to an NH<sub>2</sub> wagging fundamental. The features at 483.8 and 393.8 cm<sup>−1</sup>, with H/D ratios of 1.3962:1 and 1.2928:1 and <sup>14</sup>N/<sup>15</sup>N shifts of −0.6 and −1.9 cm<sup>−1</sup>, respectively, can be assigned to the NH<sub>2</sub> out-of-plane rock and the Al–H out-of-plane deformation modes. Unfortunately, however, the D- and <sup>15</sup>N-counterparts to the obvious candidate for the Al–H in-plane deformation mode at 482.2 cm<sup>−1</sup> were too weak to be observed.

Besides the band at 1721.8 cm<sup>−1</sup> suggesting the presence of a Ga(II)–H bond, the spectrum of **2b** also includes numerous signs of the NH<sub>2</sub> ligand. For example, the feature at 3485.4 cm<sup>−1</sup> in the spectrum of the <sup>15</sup>N isotopomer is most obviously ascribed to a ν(N–H) mode, that at 1528.7 cm<sup>−1</sup> in the spectrum of the normal isotopomer to the scissoring mode of the NH<sub>2</sub> fragment. Strong support for the second of these assignments comes not only from the H/D ratio (1.3351:1) and <sup>15</sup>N shift of −2.5 cm<sup>−1</sup>, but also from the frequencies (in cm<sup>−1</sup>) reported for the corresponding mode of the following species: HAlNH<sub>2</sub> 1533.6 (H/D = 1.3319:1), HFeNH<sub>2</sub> 1517.8 (H/D = 1.3412:1),<sup>21</sup> and HNiNH<sub>2</sub> 1533.3 (H/D = 1.3021:1).<sup>22</sup> Analogy with HAlNH<sub>2</sub> suggests that the band at 746.2 cm<sup>−1</sup> represents the NH<sub>2</sub> wagging mode of **2b**, although the H/D ratio of 1.3242:1 is rather larger than that (1.2826:1) for the aluminum compound. Evidence of <sup>69</sup>Ga/<sup>71</sup>Ga splitting and a large <sup>15</sup>N shift (−15.7 cm<sup>−1</sup>) make the feature at 668.5/667.4 cm<sup>−1</sup> the obvious candidate for a ν(Ga–N) mode. Given the conditions leading to the formation of the compound and analogies with the photochemical changes shown to occur in the systems Al/NH<sub>3</sub> and M/CH<sub>4</sub> (M = Al, Ga, or In),<sup>14</sup> the most plausible

interpretation of these properties is that **2b** is HGaNH<sub>2</sub> formed in accordance with the insertion reaction 2. The reaction energies for the formation of HMNH<sub>2</sub> by tautomerization of the ammonia adducts were calculated to be −79.6, +13.1, and +37.8 kJ mol<sup>−1</sup> for M = Al, Ga, and In, respectively.



The indium compound **2c** shows features similar to those observed for **2a** and **2b**. The absorption at 1512.9 cm<sup>−1</sup> (H/D = 1.3482:1) corresponds to the NH<sub>2</sub> scissoring mode, whereas that at 709.0 cm<sup>−1</sup> (H/D = 1.3559:1) is the obvious choice for the NH<sub>2</sub> wagging mode. There is also a signal at 564.8 cm<sup>−1</sup> which, with a <sup>15</sup>N shift of −13.1 cm<sup>−1</sup> and an H/D ratio of 1.0681:1, has the right credentials to correspond to what is mainly a ν(In–N) vibration.

DFT calculations find an equilibrium geometry with C<sub>s</sub> symmetry for each of the molecules HAlNH<sub>2</sub> and HGaNH<sub>2</sub>, as illustrated in Figure 7b. The equilibrium geometry of HInNH<sub>2</sub> exhibits only C<sub>1</sub> symmetry with the M–NH<sub>2</sub> fragment having the form of a shallow pyramid. The dimensions of all three species are given in Table 5. The H–M–N skeleton is bent with an H–M–N angle of 115.5, 116.3, or 115.5° for M = Al, Ga, or In; the M–N bonds are relatively short (measuring 1.7880, 1.8362, and 1.9929 Å for M = Al, Ga, and In, respectively).

Out of the nine IR-active vibrational fundamentals expected for each of the HMNH<sub>2</sub> molecules, no less than eight, seven, and five have been observed for HAlNH<sub>2</sub>, HGaNH<sub>2</sub>, and HInNH<sub>2</sub>, respectively, as one or other of their different isotopomers. The relative intensities, frequencies, and isotopic shifts are found to be in generally excellent agreement with the properties predicted for the optimized ground state of the molecules by DFT/B3LYP calculations. Hence, as indicated in Table 5, we have succeeded in locating and assigning all the fundamental bands in the range 420–4000 cm<sup>−1</sup> calculated to have intensities in excess of 10 km mol<sup>−1</sup>. On this basis we can confirm that the modes approximating most closely to ν(Ga–N) and ν(In–N) vibrations occur at 668.5/667.4 and 564.8 cm<sup>−1</sup>, respectively, predictably lying at lower frequency than the ν(Al–N) fundamental of HAlNH<sub>2</sub> (778.7 cm<sup>−1</sup>).

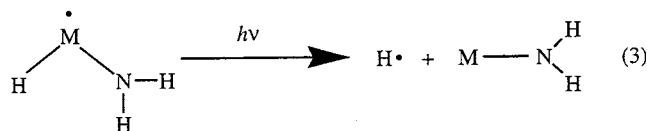
**MNH<sub>2</sub> [M = Al (3a), Ga (3b), or In (3c)].** Irradiation with broad-band UV–visible light (λ = 200–800 nm) results in the efficient conversion of HMNH<sub>2</sub> to a new product, viz., **3a** (M = Al), **3b** (M = Ga), or **3c** (M = In), which lacks any spectroscopic sign of an M–H bond. That it nevertheless retains a coordinated NH<sub>2</sub> group is implied by the observation of IR bands with frequencies and isotopic shifts appropriate to their attribution either to internal vibrations of the NH<sub>2</sub> ligand (3495.1 and 1520.3 cm<sup>−1</sup> for **3a**, 3471.6 and 1505.9 cm<sup>−1</sup> for **3b**, and 3481.7 and 1498.1 cm<sup>−1</sup> for **3c**) or to an M–N stretching vibration (726.5, 589.3/587.9, and 498.7 cm<sup>−1</sup> for **3a**, **3b**, and **3c**, respectively). The obvious inference is that **3a** is the simple aluminum(I) amide, AlNH<sub>2</sub>, and **3b** and **3c** are the corresponding gallium and indium compounds, GaNH<sub>2</sub> and InNH<sub>2</sub>, each formed by photodissociation of the M–H bond in HMNH<sub>2</sub> in accordance with reaction 3, plainly analogous to eq 1. AlNH<sub>2</sub> has been identified in an earlier matrix study<sup>19</sup> with results that match closely, but are somewhat less extensive than, the ones reported here. As with the formation of CH<sub>3</sub>M from CH<sub>3</sub>MH



**Table 5.** Comparison between the IR Spectra Observed and Calculated (Frequencies in  $\text{cm}^{-1}$ ) for  $\text{HM}^{14}\text{NH}_2/\text{HM}^{15}\text{NH}_2/\text{DM}^{14}\text{ND}_2$  (**2a–2c**) ( $\text{M} = \text{Al, Ga, or In}$ )

$\text{HM}^{14}\text{NH}_2$		$\text{HM}^{15}\text{NH}_2$		$\text{DM}^{14}\text{ND}_2$		assignment	description of vibrational mode	M
obsd	calcd <sup>a</sup>	obsd	calcd <sup>a</sup>	obsd	calcd <sup>a</sup>			
3476.4	3645.1 (14)	3468.2	3634.9 (14)	2595.6	2685.8 (11)	$\nu_1$ (a')	$\nu_{\text{sym}}(\text{N-H})$	Al
<i>b</i>	3551.1 (4)	<i>b</i>	3545.9 (4)	<i>b</i>	2568.9 (8)	$\nu_2$ (a')	$\nu_{\text{asym}}(\text{N-H})$	
1761.1	1820.5 (205)	1761.0	1820.5 (205)	1282.6	1312.0 (117)	$\nu_3$ (a')	$\nu(\text{Al-H})$	
1533.6	1620.4 (41)	1531.5	1615.1 (39)	1151.4	1208.4 (40)	$\nu_4$ (a')	$\text{NH}_2$ scissoring	
778.7	795.0 (86)	766.9	781.5 (93)	748.3	752.1 (52)	$\nu_5$ (a')	$\nu(\text{Al-N})$	
705.2	746.9 (116)	701.0	742.2 (107)	549.8	580.3 (72)	$\nu_6$ (a')	$\text{NH}_2$ wagging	
482.2	486.5 (27)	<i>b</i>	486.3 (27)	<i>b</i>	348.4 (14)	$\nu_7$ (a')	Al-H in-plane def.	
483.8	498.3 (31)	483.2	497.4 (28)	346.5	366.3 (56)	$\nu_8$ (a'')	$\text{NH}_2$ out-of-plane rock	
393.8	426.5 (226)	391.9	424.4 (227)	304.6	323.3 (94)	$\nu_9$ (a'')	Al-H out-of-plane def.	
<i>b</i>	3664.2 (14)	3485.4	3653.7 (14)	<i>b</i>	2703.3 (11)	$\nu_1$ (a')	$\nu_{\text{sym}}(\text{N-H})$	Ga
<i>b</i>	3551.5 (4)	<i>b</i>	3546.6 (4)	<i>b</i>	2566.3 (7)	$\nu_2$ (a')	$\nu_{\text{asym}}(\text{N-H})$	
1721.8	1759.3 (189)	1721.8	1759.2 (189)	1249.5	1254.3 (103)	$\nu_3$ (a')	$\nu(\text{Ga-H})$	
1528.7	1601.3 (21)	1523.2	1596.2 (20)	1145.0	1191.1 (23)	$\nu_4$ (a')	$\text{NH}_2$ scissoring	
746.2	752.2 (78)	743.7	748.1 (79)	563.5	573.8 (50)	$\nu_5$ (a')	$\text{NH}_2$ wagging	
668.5	665.0 (59)	652.8	649.3 (56)	626.6	626.8 (41)	$\nu_6$ (a')	$\nu(^{69}\text{Ga-N})$	
<i>b</i>	479.8 (6)	<i>b</i>	479.6 (6)	<i>b</i>	342.3 (5)	$\nu_7$ (a')	Ga-H in-plane def.	
494.1	481.0 (21)	494.1	481.0 (26)	<i>b</i>	342.9 (12)	$\nu_8$ (a'')	$\text{NH}_2$ out-of-plane rock	
210.9	229.1 (238)	<i>b</i>	227.6 (235)	<i>b</i>	176.6 (136)	$\nu_9$ (a'')	Ga-H out-of-plane def.	
3463.5	3597.6 (15)	<i>b</i>	3587.4 (15)	<i>b</i>	2651.8 (13)	$\nu_1$ (a)	$\nu_{\text{sym}}(\text{N-H})$	In
<i>b</i>	3486.0 (5)	<i>b</i>	3481.0 (4)	<i>b</i>	2519.4 (8)	$\nu_2$ (a)	$\nu_{\text{asym}}(\text{N-H})$	
1533.8	1580.6 (197)	1533.8	1580.0 (203)	1108.8	1121.1 (98)	$\nu_3$ (a)	$\nu(\text{In-H})$	
1512.9	1567.7 (28)	<i>b</i>	1563.5 (21)	1122.2	1162.9 (31)	$\nu_4$ (a)	$\text{NH}_2$ scissoring	
709.0	682.5 (97)	<i>b</i>	679.2 (96)	522.9	513.1 (73)	$\nu_5$ (a)	$\text{NH}_2$ wagging	
564.8	555.9 (57)	551.7	541.9 (54)	528.8	524.9 (33)	$\nu_6$ (a)	$\nu(\text{In-N})$	
<i>b</i>	407.5 (13)	<i>b</i>	407.4 (13)	<i>b</i>	290.3 (8)	$\nu_7$ (a)	$\text{NH}_2$ out-of-plane rock	
<i>b</i>	425.0 (40)	<i>b</i>	424.9 (40)	<i>b</i>	302.8 (18)	$\nu_8$ (a)	In-H in-plane def.	
<i>b</i>	154.2 (190)	<i>b</i>	153.1 (187)	<i>b</i>	119.7 (112)	$\nu_9$ (a)	In-H out-of-plane def.	

<sup>a</sup>  $\text{HAlNH}_2$  symmetry  $C_s$ : Al-H 1.6050 Å, Al-N 1.7880 Å, N-H 1.0112/1.0098 Å, H-Al-N 115.5°, Al-N-H 124.6/125.3°.  $\text{HGaNH}_2$  symmetry  $C_s$ : Ga-H 1.6019 Å, Ga-N 1.8362 Å, N-H 1.0112/1.0087 Å, H-Ga-N 116.3°, Ga-N-H 124.0/124.3°. Frequencies (in  $\text{cm}^{-1}$ ) calculated for  $\text{H}^{71}\text{Ga}^{14}\text{NH}_2$ : 3664.2 (14), 3551.5 (4), 1758.9 (189), 1601.3 (21), 752.0 (78), 663.3 (59), 479.8 (6), 480.9 (26), 229.0 (238).  $\text{HInNH}_2$  symmetry  $C_1$ : In-N 1.9929 Å, In-H 1.7676 Å, N-H 1.0178/1.0203 Å, H-In-N 115.5°, In-N-H 123.8/123.1°, H-In-N-H 15.7/172.2°. Intensities ( $\text{km mol}^{-1}$ ) are given in parentheses. <sup>b</sup> Too weak to be detected or hidden by ammonia absorptions or out of range of detection.



under similar circumstances,<sup>14</sup> the hydrogen atom expelled in this process is presumably enabled by its small size to escape from the matrix cage; it is also a potential source of secondary change.

DFT calculations have identified a global minimum corresponding to an equilibrium geometry for each of the  $\text{MNH}_2$  molecules with a planar skeleton and  $C_{2v}$  symmetry (see Figure 7c). The planar geometry at nitrogen, together with the relatively short M-N bonds in group 13 species of this type [ $r(\text{M-N}) = 1.8131, 1.8836, \text{ and } 2.0389 \text{ Å}$  for  $\text{M} = \text{Al, Ga, and In}$ , respectively], appears again to signify that N to M  $\pi$ -interactions contribute to the M-N bonding. There are therefore six distinct IR-active vibrational fundamentals spanning the representation  $3a_1 + 1b_1 + 2b_2$ . Our experiments have identified IR absorptions with frequencies, relative intensities, and isotopic shifts in good agreement with those predicted for no less than four of the fundamentals of each of the molecules  $\text{AlNH}_2$ ,  $\text{GaNH}_2$ , and  $\text{InNH}_2$ . Guided by the calculations, the isotopic shifts, and analogies with the spectra of related compounds, we arrive with some assurance at the assignments of the observed features set out in Table 6. Hence the  $\text{NH}_2$  scissoring fundamental,  $\nu_2$  ( $a_1$ ), and the M-N stretching mode,  $\nu_3$  ( $a_1$ ), are found to take the following frequencies (in  $\text{cm}^{-1}$ ):  $\text{AlNH}_2$ ,  $\nu_2 = 1520.3$ ,  $\nu_3 = 726.5$ ;  $\text{GaNH}_2$ ,  $\nu_2 = 1505.9$ ,  $\nu_3 = 589.3/587.9$ ;  $\text{InNH}_2$ ,  $\nu_2 = 1498.1$ ,  $\nu_3 = 498.7$ . When the frequencies are translated into force constants, we find that while  $f_{\text{MN}}$  maintains the order Al

$> \text{Ga} > \text{In}$ , the values are significantly smaller for the univalent species  $\text{MNH}_2$  than for the corresponding divalent one  $\text{HMNH}_2$ . This difference is also reflected in the slightly longer M-N bond distance in  $\text{MNH}_2$ . A similar pattern is displayed by the M-C bonds in the molecules  $\text{CH}_3\text{MH}$  and  $\text{CH}_3\text{M}$ , where  $\text{M} = \text{Al, Ga, or In}$ .<sup>14</sup>

**$\text{H}_2\text{MNH}_2$  [ $\text{M} = \text{Al}$  (**4a**),  $\text{Ga}$  (**4b**), or  $\text{In}$  (**4c**)].** Of the possible isomers with the composition  $\text{MNH}_4$ , that with the planar, ethene-like structure  $\text{H}_2\text{MNH}_2$  (Figure 7d) is lowest in energy by some margin, according to DFT calculations employing the B3LYP hybrid method. Details of the calculated dimensions and the corresponding vibrational frequencies are given in Table 7. The structure in each case is thus analogous to that deduced previously by both theory<sup>9</sup> and experiment<sup>8</sup> for the corresponding boron compound  $\text{H}_2\text{BNH}_2$ ; there is also good agreement with the results of earlier calculations (using, for example, SCF methods and CISD and CCSD levels of theory) taking in the aluminum compound.<sup>24,26,28</sup> The planar  $\text{H}_2\text{MNH}_2$  unit conforms to  $C_{2v}$  symmetry with the result that its 12 vibrational fundamentals are accommodated by the representation  $5a_1 + 1a_2 + 2b_1 + 4b_2$ . Of the 11 IR-active modes ( $5a_1 + 2b_1 + 4b_2$ ), all but two have been satisfactorily identified in the spectra measured for  $\text{H}_2\text{AlNH}_2$  (**4a**) and all but one have been so identified in the spectra measured for  $\text{H}_2\text{GaNH}_2$  (**4b**). In these two cases the transitions that have escaped detection have probably been obscured by more intense absorptions due to the other molecules present in the matrices. Only with  $\text{H}_2\text{InNH}_2$ , invariably formed in low concentrations, are the observed transitions exceeded in number by the unobserved ones, mainly for want of intensity but partly also for reasons of frequency

**Table 6.** Comparison between the IR Spectra Observed and Calculated (Frequencies in cm<sup>-1</sup>) for M<sup>14</sup>NH<sub>2</sub>/M<sup>15</sup>NH<sub>2</sub>/M<sup>14</sup>ND<sub>2</sub> (**3a–3c**) (M = Al, Ga, or In)

M <sup>14</sup> NH <sub>2</sub>		M <sup>15</sup> NH <sub>2</sub>		M <sup>14</sup> ND <sub>2</sub>		assignment	description of vibrational mode	M
obsd	calcd <sup>a</sup>	obsd	calcd <sup>a</sup>	obsd	calcd <sup>a</sup>			
<i>b</i>	3503.7 (0.06)	<i>b</i>	3498.6 (0.15)	<i>b</i>	2534.6 (2)	$\nu_1$ (a <sub>1</sub> )	$\nu_{\text{sym}}(\text{N-H})$	Al
1520.3	1614.0 (63)	1515.0	1608.7 (60)	1137.8	1202.6 (64)	$\nu_2$ (a <sub>1</sub> )	NH <sub>2</sub> scissoring	
726.5	735.1 (81)	713.6	721.9 (79)	694.9	698.2 (64)	$\nu_3$ (a <sub>1</sub> )	$\nu(\text{Al-N})$	
406.5	469.3 (263)	403.9	466.2 (260)	314.6	364.7 (149)	$\nu_4$ (b <sub>1</sub> )	out-of-plane def.	
3495.1	3590.3 (6)	3486.2	3580.4 (6)	<i>b</i>	2643.5 (3)	$\nu_5$ (b <sub>2</sub> )	$\nu_{\text{asym}}(\text{N-H})$	
<i>b</i>	499.0 (0.1)	<i>b</i>	496.8 (0.1)	<i>b</i>	377.4 (0.01)	$\nu_6$ (b <sub>2</sub> )	$\rho(\text{NH}_2)$	
<i>b</i>	3499.8 (1)	<i>b</i>	3494.2 (0.7)	<i>b</i>	2528.7 (1)	$\nu_1$ (a <sub>1</sub> )	$\nu_{\text{sym}}(\text{N-H})$	Ga
1505.9	1599.9 (32)	1501.2	1595.0 (30)	1132.6	1189.5 (40)	$\nu_2$ (a <sub>1</sub> )	NH <sub>2</sub> scissoring	
589.3	595.2 (94)	574.3	581.0 (89)	557.9	560.8 (78)	$\nu_3$ (a <sub>1</sub> )	$\nu(^{69}\text{Ga-N})$	
303.3	363.5 (283)	302.7	362.7 (280)	<i>b</i>	282.5 (164)	$\nu_4$ (b <sub>1</sub> )	out-of-plane def.	
3471.6	3599.7 (2)	<i>b</i>	3588.7 (3)	<i>b</i>	2652.1 (1)	$\nu_5$ (b <sub>2</sub> )	$\nu_{\text{asym}}(\text{N-H})$	
<i>b</i>	509.0 (1)	<i>b</i>	507.3 (1)	<i>b</i>	382.4 (0.4)	$\nu_6$ (b <sub>2</sub> )	$\rho(\text{NH}_2)$	
<i>b</i>	3446.0 (0.5)	<i>b</i>	3441.2 (1)	<i>b</i>	2490.6 (1)	$\nu_1$ (a <sub>1</sub> )	$\nu_{\text{sym}}(\text{N-H})$	In
1498.1	1568.1 (26)	1493.6	1563.3 (24)	1116.3	1160.8 (33)	$\nu_2$ (a <sub>1</sub> )	NH <sub>2</sub> scissoring	
498.7	504.3 (93)	488.2	491.3 (89)	480.6	475.3 (80)	$\nu_3$ (a <sub>1</sub> )	$\nu(\text{In-N})$	
237.0	256.3 (236)	235.4	254.6 (233)	<i>b</i>	198.3 (139)	$\nu_4$ (b <sub>1</sub> )	out-of-plane def.	
3481.7	3548.3 (4)	<i>b</i>	3538.4 (4)	<i>b</i>	2613.3 (3)	$\nu_5$ (b <sub>2</sub> )	$\nu_{\text{asym}}(\text{N-H})$	
469.6	447.8 (3)	<i>b</i>	445.9 (3)	<i>b</i>	335.1 (1)	$\nu_6$ (b <sub>2</sub> )	$\rho(\text{NH}_2)$	

<sup>a</sup> AlNH<sub>2</sub> symmetry  $C_{2v}$ : Al–N 1.8131 Å, N–H 1.0149 Å, H–N–H 108.5°. GaNH<sub>2</sub> symmetry  $C_{2v}$ : Ga–N 1.8836 Å, N–H 1.0145 Å, H–N–H 109.3°. Frequencies (in cm<sup>-1</sup>) calculated for <sup>71</sup>GaNH<sub>2</sub>: 3598.9 (3), 3499.1 (0.5), 1600.2 (32), 593.5 (93), 509.4 (1), 365.9 (283). InNH<sub>2</sub> symmetry  $C_{2v}$ : In–N 2.0389 Å, N–H 1.0227 Å, H–N–H 107.9°. Intensities (km mol<sup>-1</sup>) are given in parentheses. <sup>b</sup> Too weak to be detected or hidden by ammonia absorptions.

(i.e., outside the experimental limits of 4000–200 cm<sup>-1</sup>) or of masking by the absorptions of other species.

The calculated frequencies and relative intensities have then played a central role in guiding the assignment of the IR absorptions displayed by the molecules **4a–4c**. Validation of the proposed assignments comes mainly from the measured isotopic shifts, with supporting evidence being provided by analogies with the vibrational properties already established for related molecules [e.g., MH<sub>3</sub> (M = Al, Ga, or In),<sup>10</sup> H<sub>2</sub>MCl (M = Ga<sup>42</sup> or In<sup>15</sup>), HMNH<sub>2</sub>, and MNH<sub>2</sub> (M = Al, Ga, or In)]. The ability of the calculations to reproduce the frequencies (with rms deviations of no more than 3.3 and 5.8% for **4a** and **4b**, respectively), isotopic shifts, and intensity patterns of the observed spectra would appear to confirm the identities and geometries of the aluminum and gallium compounds, with strong circumstantial grounds for presuming that in the compound **4c** indium follows suit. Best defined by its measured vibrational properties is the gallium compound, **4b**, and just how well experiment generally matches theory may be gauged by the <sup>15</sup>N shifts (all negative and in cm<sup>-1</sup>) displayed by the following bands (with frequencies also in cm<sup>-1</sup>) presented in parentheses in the order exptl/calcd: 3510.7 (10.0/10.8), 3413.4 (7.5/4.9), 1970.8 (0.1/0.1), 1530.4 (6.1/5.4), 782.8 (4.5/4.7), 779.6 (4.4/3.5), 706.2/704.1 (14.0/13.1), 567.7 (0.3/0.0), and 304.9 (2.1/2.4). In addition, the observed <sup>69</sup>Ga/<sup>71</sup>Ga splitting of 2.1 cm<sup>-1</sup> characterizing the absorption near 705 cm<sup>-1</sup> matches admirably the calculated value of 1.9 cm<sup>-1</sup> for what is essentially the  $\nu(\text{Ga-N})$  mode,  $\nu_5$  (a<sub>1</sub>).

Two of the most prominent bands due to H<sub>2</sub>AlNH<sub>2</sub>—at 1899.3 and 1891.0 cm<sup>-1</sup>—tally with features reported by Lanzisera and Andrews<sup>19</sup> in the course of their matrix studies of the reactions between laser-ablated Al atoms and NH<sub>3</sub>. On that occasion they were assigned somewhat tentatively not to H<sub>2</sub>AlNH<sub>2</sub> but to the nonlinear, high-energy isomer of AlNH<sub>2</sub>, namely, HAlNH. Laser ablation produces highly energetic Al atoms, including some that are electronically excited, and the odds are that the compound **4a** would be formed, at least as a minor product, in the earlier experiments. With no less than nine IR bands now traceable to this species, including several features characteristic of an NH<sub>2</sub> group, it would be hard to

reconcile our observations with HAlNH, a molecule having the potential for no more than six distinct IR-active fundamentals. Nevertheless, we have extended our DFT calculations to include molecules of the type HMNH (M = Al, Ga, or In), thereby securing the optimum geometry illustrated in Figure 7e. Hence we confirm that such molecules are indeed high-energy species, being less stable than MNH<sub>2</sub> by 177.7, 188.4, and 257.5 kJ mol<sup>-1</sup> for M = Al, Ga, and In, respectively. The geometries are invariably bent, with H–M–N angles near 160° and M–N–H angles near 120°, although the potential well is extremely shallow with respect to the bending coordinates. Despite the absence of the conventional signs of multiple  $\pi$ -bonding, the M–N bond is calculated (at 1.6271, 1.6989, and 1.8345 Å for M = Al, Ga, and In, respectively) to be shorter than in any other compound with the general formula MNH<sub>*n*</sub> (*n* = 2–6). The most distinctive feature of the vibrational properties is the high frequency of the  $\nu(\text{M-H})$  fundamental, which is predicted, for example, to be about 100 cm<sup>-1</sup> higher for HAlNH than for the corresponding modes of H<sub>2</sub>AlNH<sub>2</sub>. Hence a frequency near 2000 cm<sup>-1</sup>, rather than 1900 cm<sup>-1</sup>, as observed for **4a**, is to be expected for HAlNH. On the evidence of published work, therefore, we are doubtful whether this molecule, or any homologue of the heavier group 13 metals, has yet been sighted in the laboratory.

The signal at 1887.6 cm<sup>-1</sup> in the experiments with Al and those at 1942.0 and 754.3 cm<sup>-1</sup> in the experiments with Ga can be assigned either to an ammonia adduct of H<sub>2</sub>MNH<sub>2</sub> or to the dimer [H<sub>2</sub>MNH<sub>2</sub>]<sub>2</sub>. To gain more information about the possible dimerization 2H<sub>2</sub>MNH<sub>2</sub> → [H<sub>2</sub>MNH<sub>2</sub>]<sub>2</sub> for M = Al or Ga, we have calculated the reaction energy, as well as the structure and IR spectra of the dimer. In each case, the dimer has a structure with  $D_{2h}$  symmetry and two bridging NH<sub>2</sub> units (bond length in Å, angles in deg: [H<sub>2</sub>AlNH<sub>2</sub>]<sub>2</sub> Al–H 1.5896, Al–N 1.9808, N–H 1.0162, Al···Al 2.8712, H–Al–H 123.3, N–Al–N 87.1, H–N–H 106.4; [H<sub>2</sub>GaNH<sub>2</sub>]<sub>2</sub> Ga–H 1.5710, Ga–N 2.0373, N–H 1.0152, Ga···Ga 2.9885, H–Ga–H 125.2, N–Ga–N 85.6, H–N–H 106.7). Both processes are exothermic with reaction energies of 197.1 kJ mol<sup>-1</sup> for Al and 240.6 kJ mol<sup>-1</sup> for Ga, much higher than the estimated energy for the formation of Ga<sub>2</sub>H<sub>6</sub> from two GaH<sub>3</sub> molecules (92.8 kJ

**Table 7.** Comparison between the IR Spectra Observed and Calculated (Frequencies in  $\text{cm}^{-1}$ ) for  $\text{H}_2\text{M}^{14}\text{NH}_2/\text{H}_2\text{M}^{15}\text{NH}_2/\text{D}_2\text{M}^{14}\text{ND}_2$  (**4a–4c**) (M = Al, Ga, or In)

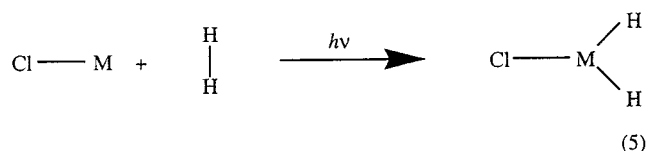
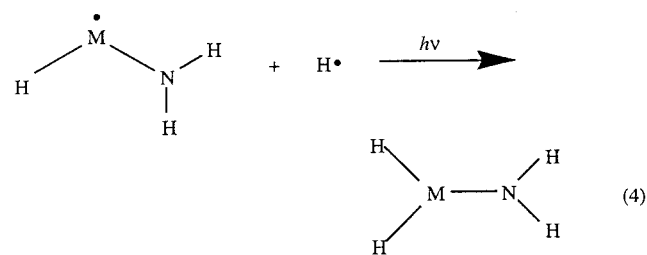
$\text{H}_2\text{M}^{14}\text{NH}_2$		$\text{H}_2\text{M}^{15}\text{NH}_2$		$\text{D}_2\text{M}^{14}\text{ND}_2$		assignment	description of vibrational mode	M
obsd	calcd <sup>a</sup>	obsd	calcd <sup>a</sup>	obsd	calcd <sup>a</sup>			
3499.7	3572.0 (11)	<i>b</i>	3566.9 (10)	<i>b</i>	2583.9 (13)	$\nu_1$ (a <sub>1</sub> )	$\nu_{\text{sym}}(\text{N–H})$	Al
1891.0	1959.3 (81)	1891.1	1959.3 (81)	<i>b</i>	1398.2 (58)	$\nu_2$ (a <sub>1</sub> )	$\nu_{\text{sym}}(\text{Al–H})$	
1541.6	1631.2 (49)	1536.1	1625.8 (47)	1159.5	1218.0 (46)	$\nu_3$ (a <sub>1</sub> )	$\delta(\text{NH}_2)$	
818.7	830.1 (192)	809.8	820.2 (214)	<i>b</i>	774.1 (72)	$\nu_4$ (a <sub>1</sub> )	$\nu(\text{Al–N})$	
755.0	754.6 (86)	<i>b</i>	749.6 (63)	548.4	548.7 (86)	$\nu_5$ (a <sub>1</sub> )	$\delta(\text{AlH}_2)$	
	499.9 (0)		499.9 (0)		353.6 (0)	$\nu_6$ (a <sub>2</sub> )	twist	
608.7	608.4 (150)	608.1	608.4 (149)	450.4	455.5 (124)	$\nu_7$ (b <sub>1</sub> )	$\rho_{\text{out-of-plane}}(\text{AlH}_2)$	
518.3	483.0 (309)	516.7	479.6 (306)	397.7	376.9 (149)	$\nu_8$ (b <sub>1</sub> )	$\rho_{\text{out-of-plane}}(\text{NH}_2)$	
<i>b</i>	3655.8 (11)	<i>b</i>	3645.5 (11)	<i>b</i>	2694.5 (11)	$\nu_9$ (b <sub>2</sub> )	$\nu_{\text{asym}}(\text{N–H})$	
1899.3	1964.2 (288)	1899.3	1964.2 (288)	1384.2	1426.6 (169)	$\nu_{10}$ (b <sub>2</sub> )	$\nu_{\text{asym}}(\text{Al–H})$	
769.8	767.6 (151)	766.2	762.9 (150)	611.0	603.4 (88)	$\nu_{11}$ (b <sub>2</sub> )	$\delta_{\text{in-plane}}(\text{NH}_2)$	
<i>b</i>	433.5 (22)	<i>b</i>	433.5 (22)	<i>b</i>	311.7 (10)	$\nu_{12}$ (b <sub>2</sub> )	$\delta_{\text{in-plane}}(\text{AlH}_2)$	
3413.4	3581.9 (9)	3405.9	3577.0 (9)	<i>b</i>	2588.3 (11)	$\nu_1$ (a <sub>1</sub> )	$\nu_{\text{sym}}(\text{N–H})$	Ga
1970.8	1995.9 (64)	<i>b</i>	1995.9 (64)	1407.7	1415.6 (33)	$\nu_2$ (a <sub>1</sub> )	$\nu_{\text{sym}}(\text{Ga–H})$	
1530.4	1621.6 (30)	1524.3	1616.2 (28)	1150.9	1208.6 (30)	$\nu_3$ (a <sub>1</sub> )	$\delta(\text{NH}_2)$	
779.6	740.3 (40)	775.2	736.8 (59)	568.8	519.8 (68)	$\nu_4$ (a <sub>1</sub> )	$\delta(\text{GaH}_2)$	
706.2	689.0 (124)	692.2	675.9 (103)	667.8	658.0 (21)	$\nu_5$ (a <sub>1</sub> )	$\nu(^{69}\text{Ga–N})$	
	545.8 (0)		545.8 (0)		386.1 (0)	$\nu_6$ (a <sub>2</sub> )	twist	
567.7	607.9 (43)	567.4	607.9 (43)	405.9	439.7 (26)	$\nu_7$ (b <sub>1</sub> )	$\rho_{\text{out-of-plane}}(\text{GaH}_2)$	
304.9	337.3 (280)	302.8	334.9 (277)	<i>b</i>	263.3 (161)	$\nu_8$ (b <sub>1</sub> )	$\rho_{\text{out-of-plane}}(\text{NH}_2)$	
3510.7	3681.7 (13)	3500.7	3670.9 (12)	<i>b</i>	2717.3 (12)	$\nu_9$ (b <sub>2</sub> )	$\nu_{\text{asym}}(\text{N–H})$	
1970.8	1998.6 (245)	1970.7	1998.5 (245)	1419.1	1428.3 (133)	$\nu_{10}$ (b <sub>2</sub> )	$\nu_{\text{asym}}(\text{Ga–H})$	
782.8	789.8 (110)	778.3	785.1 (109)	605.1	608.8 (64)	$\nu_{11}$ (b <sub>2</sub> )	$\delta_{\text{in-plane}}(\text{NH}_2)$	
<i>b</i>	441.8 (26)	<i>b</i>	441.7 (27)	<i>b</i>	316.2 (12)	$\nu_{12}$ (b <sub>2</sub> )	$\delta_{\text{in-plane}}(\text{GaH}_2)$	
<i>b</i>	3517.1 (10)	<i>b</i>	3512.3 (9)	<i>b</i>	2541.6 (12)	$\nu_1$ (a <sub>1</sub> )	$\nu_{\text{sym}}(\text{N–H})$	In
<i>b</i>	1770.2 (68)	<i>b</i>	1770.2 (68)	<i>b</i>	1254.1 (38)	$\nu_2$ (a <sub>1</sub> )	$\nu_{\text{sym}}(\text{In–H})$	
1506.6	1579.4 (23)	<i>b</i>	1574.5 (22)	<i>b</i>	1171.3 (24)	$\nu_3$ (a <sub>1</sub> )	$\delta(\text{NH}_2)$	
<i>b</i>	634.2 (84)	<i>b</i>	631.4 (106)	474.6	441.7 (110)	$\nu_4$ (a <sub>1</sub> )	$\delta(\text{InH}_2)$	
616.3	575.8 (153)	599.2	563.4 (128)	<i>b</i>	553.4 (28)	$\nu_5$ (a <sub>1</sub> )	$\nu(\text{In–N})$	
	480.8 (0)		480.8 (0)		340.1 (0)	$\nu_6$ (a <sub>2</sub> )	twist	
<i>b</i>	535.2 (95)	<i>b</i>	535.2 (94)	<i>b</i>	384.0 (52)	$\nu_7$ (b <sub>1</sub> )	$\rho_{\text{out-of-plane}}(\text{InH}_2)$	
<i>c</i>	177.6 (237)	<i>c</i>	176.3 (234)	<i>c</i>	139.5 (140)	$\nu_8$ (b <sub>1</sub> )	$\rho_{\text{out-of-plane}}(\text{NH}_2)$	
<i>b</i>	3621.9 (18)	<i>b</i>	3611.5 (17)	<i>b</i>	2671.3 (17)	$\nu_9$ (b <sub>2</sub> )	$\nu_{\text{asym}}(\text{N–H})$	
1805.9	1756.9 (272)	1805.9	1756.9 (272)	1299.0	1250.7 (141)	$\nu_{10}$ (b <sub>2</sub> )	$\nu_{\text{asym}}(\text{In–H})$	
733.3	696.3 (126)	731.4	692.2 (125)	<i>b</i>	534.1 (76)	$\nu_{11}$ (b <sub>2</sub> )	$\delta_{\text{in-plane}}(\text{NH}_2)$	
<i>b</i>	368.5 (33)	<i>b</i>	368.4 (34)	<i>b</i>	263.3 (16)	$\nu_{12}$ (b <sub>2</sub> )	$\delta_{\text{in-plane}}(\text{InH}_2)$	

<sup>a</sup>  $\text{H}_2\text{AlNH}_2$  symmetry  $C_{2v}$ : Al–N 1.7790 Å, Al–H 1.5811 Å, N–H 1.0100 Å, H–Al–H 124.4°, H–N–H 110.0°.  $\text{H}_2\text{GaNH}_2$  symmetry  $C_{2v}$ : Ga–N 1.8211 Å, Ga–H 1.5621 Å, N–H 1.0086 Å, H–Ga–H 126.7°, H–N–H 111.7°. Frequencies (in  $\text{cm}^{-1}$ ) calculated for  $\text{H}_2^{71}\text{GaNH}_2$ : 3681.7 (13), 3581.9 (9), 1998.0 (242), 1995.8 (67), 1621.6 (30), 789.5 (110), 740.2 (41), 687.1 (122), 607.5 (42), 545.8 (0), 441.7 (26), 337.2 (278).  $\text{H}_2\text{InNH}_2$  symmetry  $C_{2v}$ : In–N 1.9703 Å, In–H 1.7252 Å, N–H 1.0169 Å, H–In–H 126.9°, H–N–H 110.3°. Intensities ( $\text{km mol}^{-1}$ ) are given in parentheses. <sup>b</sup> Too weak to be detected or hidden by ammonia absorptions. <sup>c</sup> Out of range of detection.

$\text{mol}^{-1}$ ). However, as for the dimerization of  $\text{GaH}_3$ , a substantial reaction barrier is likely to prohibit the reaction in a solid argon matrix. The calculations gave the following frequencies for the most intense IR absorptions [values in  $\text{cm}^{-1}$  with intensities ( $\text{km mol}^{-1}$ ) in brackets]:  $[\text{H}_2\text{AlNH}_2]_2$  1922.3 (634)  $b_{1u}$ , 1915.0 (230)  $b_{3u}$ , 901.1 (613)  $b_{3u}$ , 763.1 (214)  $b_{1u}$ , 762.3 (651)  $b_{2u}$ , 738.0 (421)  $b_{3u}$ ;  $[\text{H}_2\text{GaNH}_2]_2$  1958.2 (548)  $b_{1u}$ , 1949.7 (274)  $b_{3u}$ , 894.7 (334)  $b_{3u}$ , 720.1 (250)  $b_{3u}$ , 717.1 (165)  $b_{1u}$ , 702.5 (347)  $b_{2u}$ . Annealing the matrices did not lead to a significant change in the intensities of any signals. The observation of the absorptions at 1887.6, 1942.0, and  $754.3 \text{ cm}^{-1}$  even at low metal concentrations seems therefore to favor their assignment to the ammonia adducts  $\text{H}_2\text{MNH}_2 \cdot \text{NH}_3$ .

**Origins of the Products 4a–4c.** While the origins of  $\text{M} \cdot \text{NH}_3$ ,  $\text{HMNH}_2$ , and  $\text{MNH}_2$ , the primary products of the thermal and photochemical reactions occurring between a group 13 metal atom M and  $\text{NH}_3$ , are relatively clear, the reaction or reactions affording the secondary product  $\text{H}_2\text{MNH}_2$  are less obvious. One mechanism involves the addition of the H atoms released in the photoreaction 3 to the subvalent metal compounds  $\text{MNH}_2$  and  $\text{HMNH}_2$ , as in eq 4, for example. However, the knowledge that  $\text{H}_2$  molecules undergo photoactivated addition to  $\text{GaCl}^{42}$  or  $\text{InCl}^{15}$  (eq 5) to give the trivalent product  $\text{H}_2\text{MCl}$  (M = Ga or In) suggests an alternative mechanism in which a similar

reaction is induced between  $\text{H}_2$  (formed by recombination of the H atoms) and the univalent metal amide  $\text{MNH}_2$ . Investigation of this second possibility was the primary motive for carrying out experiments in which the matrices were doped with both ammonia and dihydrogen. The addition of  $\text{H}_2$  was certainly found to boost the yield of  $\text{H}_2\text{MNH}_2$ . Although this might seem to favor the second mechanism involving largely concerted photoaddition of  $\text{H}_2$  to  $\text{MNH}_2$ , the presence of  $\text{H}_2$  led also to the formation of the dihydride  $\text{MH}_2$  and thence, on broad-band UV–visible photolysis, to the monohydride  $\text{MH}$  and H atoms;<sup>10</sup> it therefore provides an additional source of H atoms. Telling evidence that H atoms and not  $\text{H}_2$  are the principal, possibly sole, means of access to  $\text{H}_2\text{MNH}_2$  comes from an experiment involving a matrix containing Ga atoms together with  $\text{NH}_3$  and  $\text{D}_2$ . Were  $\text{D}_2$  addition the primary reaction, the main product would be  $\text{D}_2\text{GaNH}_2$  readily recognizable by the strong IR absorptions near  $1400 \text{ cm}^{-1}$  due to its  $\nu(\text{Ga–D})$  modes. In the event, only weak absorptions were observed to build up in this region, whereas relatively strong bands were observed to develop near  $1970 \text{ cm}^{-1}$  (indicating that cleavage of an N–H bond is more readily achieved than cleavage of a D–D bond). It was also apparent that the yield of  $\text{H}_2\text{GaNH}_2$  decreased almost to vanishing point when the matrix concentration of  $\text{NH}_3$  was reduced by a factor of 10. Hence we conclude that H atoms



produced by broad-band UV–visible photolysis of HMNH<sub>2</sub> are the main begetters of H<sub>2</sub>MNH<sub>2</sub> in a reaction sequence that plainly requires the activation of more than one NH<sub>3</sub> molecule.

### Conclusions

The reactions that occur between Al, Ga, or In atoms and NH<sub>3</sub> have been investigated using the technique of matrix isolation to trap both the reagents and products and investigate their photochemistries. The various products have been identified and characterized primarily by their IR spectra. The response of the spectra to replacing <sup>14</sup>NH<sub>3</sub> by <sup>14</sup>ND<sub>3</sub> or <sup>15</sup>NH<sub>3</sub> and to the natural presence of <sup>69</sup>Ga and <sup>71</sup>Ga and the vibrational properties simulated for the individual molecules by DFT calculations have played central roles in assessing the natures of these products.

The first product formed by the thermal reaction of the metal atoms with NH<sub>3</sub> is the adduct M•NH<sub>3</sub> (M = Al, Ga, or In), which can be identified not only by its IR spectrum but also by a visible absorption band near 428 nm for Al/NH<sub>3</sub>, near 440

nm for Ga/NH<sub>3</sub>, and near 435 nm for In/NH<sub>3</sub>. Irradiation with visible light having  $\lambda = \text{ca. } 436 \text{ nm}$  brings about tautomerization of M•NH<sub>3</sub> with insertion of the metal atom into one of the N–H bonds of ammonia to form the odd-electron amidometal hydride, HMNH<sub>2</sub>. As in the reactions with H<sub>2</sub><sup>10</sup> and CH<sub>4</sub>,<sup>14</sup> this change appears to be contingent on excitation of the metal atom from its ground <sup>2</sup>P to a <sup>2</sup>S or <sup>2</sup>D state; the visible absorption of the adduct probably represents the <sup>2</sup>S ← <sup>2</sup>P transition of the coordinated M atom. The M(II) derivatives suffer photodissociation under the action of broad-band UV–visible light (200 ≤  $\lambda$  ≤ 800 nm) with the formation of the univalent metal amide, MNH<sub>2</sub>, and the release of H atoms. A secondary reaction brought about by these atoms involves addition to MNH<sub>2</sub> or HMNH<sub>2</sub> to produce trivalent amidoalane, -gallane or -indane, H<sub>2</sub>MNH<sub>2</sub> (M = Al, Ga, or In). The H<sub>2</sub>MNH<sub>2</sub> molecules are characterized by planar, ethene-like geometries with C<sub>2v</sub> symmetry. The calculated M–N bond lengths follow the order M•NH<sub>3</sub> > H<sub>3</sub>M•NH<sub>3</sub> > MNH<sub>2</sub> > HMNH<sub>2</sub> ≥ H<sub>2</sub>MNH<sub>2</sub> > HMNH. As reported previously,<sup>30</sup> the barriers to rotation about the MN bond of H<sub>2</sub>MNH<sub>2</sub> are calculated to be 161.9, 50.6, 65.7, and 51.5 kJ mol<sup>−1</sup> for M = B, Al, Ga, and In, respectively, implying that  $\pi$ -interactions play quite a minor role in molecules of this sort, except when M = B. A fuller discussion of the observed and calculated properties of MNH<sub>*n*</sub> molecules (*n* = 0–6), addressing inter alia the influences of  $\pi$ -bonding and bond polarity, will be presented elsewhere.<sup>47</sup>

**Acknowledgment.** The authors thank (i) the EPSRC for support of this research, including the purchase of equipment and the award of an Advanced Fellowship to T.M.G., and (ii) the Deutsche Forschungsgemeinschaft for the award of a postdoctoral grant to H.-J.H.

JA001313X

(47) Himmel, H.-J.; Downs, A. J.; Greene, T. M. *J. Chem. Soc., Dalton Trans.*, manuscript in preparation.